

Review

Light-Induced Advanced Oxidation Processes as PFAS Remediation Methods: A Review

Domenico Leonello ¹, Murilo Alexandre Fendrich ¹, Francesco Parrino ², Nainesh Patel ³, Michele Orlandi ¹ and Antonio Miotello ^{1,*}

¹ Department of Physics, University of Trento, Via Sommarive 14, 38123 Trento, Italy; domenico.leonello@studenti.unitn.it (D.L.); murilo.fendrich@unitn.it (M.A.F.); michele.orlandi@unitn.it (M.O.)

² Department of Industrial Engineering, University of Trento, Via Sommarive 9, 38123 Trento, Italy; francesco.parrino@unitn.it

³ Department of Physics and Electronics, Christ University, Bengaluru 560029, India; nainesh11@gmail.com

* Correspondence: antonio.miotello@unitn.it

Abstract: PFAS substances, which have been under investigation in recent years, are certainly some of the most critical emerging contaminants. Their presence in drinking water, correlated with diseases, is consistently being confirmed by scientific studies in the academic and health sectors. With the aim of developing new technologies to mitigate the water contamination problem, research activity based on advanced oxidation processes for PFAS dealkylation and subsequent mineralization is active. While UV radiation could be directly employed for decontamination, there are nevertheless considerable problems regarding its use, even from a large-scale perspective. In contrast, the use of cheap, robust, and green photocatalytic materials active under near UV-visible radiation shows interesting prospects. In this paper we take stock of the health problems related to PFAS, and then provide an update on strategies based on the use of photocatalysts and the latest findings regarding reaction mechanisms. Finally, we detail some brief considerations in relation to the economic aspects of possible solutions.

Keywords: PFAS substances; emerging contaminants; water decontamination; photocatalysts; advanced oxidation processes

Citation: Leonello, D.; Fendrich, M.A.; Parrino, F.; Patel, N.; Orlandi, M.; Miotello, A.; Light-Induced Advanced Oxidation Processes as PFAS Remediation Methods: A Review. *Appl. Sci.* **2021**, *11*, 8458. <https://doi.org/10.3390/app11188458>

Academic Editor: Roberto Zivieri

Received: 30 July 2021

Accepted: 9 September 2021

Published: 12 September 2021

Publisher's Note: MDPI stays neutral with regard to jurisdictional claims in published maps and institutional affiliations.



Copyright: © 2021 by the authors. Licensee MDPI, Basel, Switzerland. This article is an open access article distributed under the terms and conditions of the Creative Commons Attribution (CC BY) license (<https://creativecommons.org/licenses/by/4.0/>).

1. Introduction

Per- and poly-fluoroalkyl substances (PFASs) are highly fluorinated aliphatic compounds in which the hydrogen atoms are partially or totally replaced by fluorine atoms, resulting in the perfluoroalkyl moiety C_nF_{2n+1} [1]. PFAS compounds are employed worldwide due to their outstanding chemical and physical properties: they are highly stable and show both hydrophobic and lipophobic functionalities. Applications include paintings, clothing, electrical conductors, Teflon[®] coatings and fluorotelomer production, firefighting foams, paper packaging products, and cookware. Among the most employed PFAS products are perfluorooctanoic (PFOA) and perfluorooctanesulfonic (PFOS) acid [2,3].

Nevertheless, PFASs are also reported to be persistent and bio-accumulative organic pollutants that are extremely toxic to living beings, with continuous exposure increasingly documented as the leading cause of adverse outcomes in humans such as immunotoxicity, hepatotoxicity, and carcinogenicity [4]. Moreover, these substances have been detected in a wide variety of samples including seawater, drinking water, ground water, indoor dust, plants, and the blood of humans and wildlife [5]. Due to the mounting evidence on dangerous effects and the still uncertain efficacy of treatment methods, PFASs are classified as contaminants of emerging concern (CEC), in addition to being

considered as “forever chemicals”. Once in the human blood, their elimination can require from months to years [6].

In recent years, different technologies have been developed aiming to purify water contaminated with PFAS compounds. Photolysis has been considered but given the C-F bond strength of around 480 kJ/mol [7], impractical wavelengths shorter than 250 nm are needed to drive efficient cleavage.

Physical adsorption and redox process have been also investigated. Physical adsorption processes using powdered activated carbon (PAC) and granulated activated carbon (GAC) are the most studied and used techniques for PFAS removal from water. These techniques present the limitation of only transferring PFAS molecules from one medium to another, and therefore require further treatments downstream [5].

In this respect, redox processes present potential advantages towards PFAS degradation, enforcing continuous defluorination of the chain and thus featuring degradation to shorter and safer molecules and ultimately to mineralization [1,3,8]. Several efforts to develop cost-effective photocatalytic pathways are currently under investigation, although the overall photocatalytic defluorination and degradation mechanisms are quite complex and still need to be detailed. Novel photocatalytic materials in combination with various illumination sources have been tested for PFAS degradation, with relevant results. High degradation and defluorination efficiencies were achieved in neutral pH conditions, with photocatalyst materials (such as In_2O_3 nanoporous nanospheres [9,10] and Ga_2O_3 needle- and sheaf-like nanostructures [11]) which have drawbacks in terms of biocompatibility, availability, and cost. So far, the most likely solutions rely on the use of either $\text{Fe}^{2+}/\text{H}_2\text{O}_2$ or TiO_2/O_3 combined with UV light under acidic pH [5].

The challenge here relies on the development of low-toxicity, efficient, and cost-effective materials preferably featuring an optical energy gap compatible with the near UV-visible range (between 350 and 500 nm), therefore providing the possibility of employing lower-cost radiation sources such as artificial visible light illumination, or concentrated sunlight, a clean and renewable resource.

In this review, an analysis of current literature on the applications of advanced oxidation processes for PFAS remediation in water is proposed, focusing on the materials and methods employed with an eye on economic viability. This report starts with a brief overview of PFAS applications and environmental and health concerns, as well as a comparison of conventional vs. emerging treatment methods and related analytical techniques. An extensive review is then presented on light-induced treatment methods (including photolysis), with an update on direct or sacrificial-mediated photocatalysis, materials, methods, and the corresponding reaction mechanisms. Finally, an overview of the employed radiation sources and an economic analysis provides a perspective on possible future outcomes for PFAS treatments as well as costs and efficiencies.

2. PFAS Applications and Related Concerns

2.1. What Are PFASs Used for?

PFASs can be divided into two main classes: polymers and non-polymers [12]. The most famous example of a non-polymer and one of the most employed PFASs is PFOA, used as a surfactant in the emulsion polymerization of fluoropolymers and as a building block for the synthesis of perfluoroalkyl-substituted compounds, polymers, and polymeric materials, with Teflon® being the most-well known example [13]. Fluorotelomer-based products (non-polymer PFASs) have been shown to degrade to PFOA over periods of decades, and thus they are a huge source of PFOA in the environment [14]. Generally, PFAS release at industrial facilities occurs through wastewater and stormwater discharge, on- and off-site disposal of solid waste, accidental releases through leaks and spills, and stack and fugitive emissions. Stack emissions may result in the aerial deposition of PFAS into soil and surface water (with subsequent

leaching and infiltration to groundwater) related to the facility, as well as short- and long-range air transport of PFAS [3]. In a recent study, more than 200 applications in 64 categories identified nearly 1400 individual types of PFASs supplied by 21 industry branches. Among the use categories, medical instruments, the photographic industry, the semiconductor industry, coatings, paints and varnishes, fire-fighting foams, and printing are the largest employment categories, with more than 100 identified PFASs [15].

2.2. Reasons for Concern

So far, a substantial number of studies have proved many adverse effects of PFASs on human health. PFOS and PFOA, at concentrations of the order of few micrograms per liter in blood, may cause hypercholesterolemia, ulcerative colitis, thyroid disease, cancer, pregnancy-induced hypertension, pre-eclampsia, and liver damage. For each of these outcomes, a molecular mechanism has been tentatively proposed. In this regard, one of the most comprehensive collections of epidemiological studies linking adverse human health effects and many other problems to PFASs (particularly PFOA) is still under investigation and is authored by the C8 Science Panel [4,16]. Figure 1 summarizes the diseases already confirmed to be associated with PFAS substances.

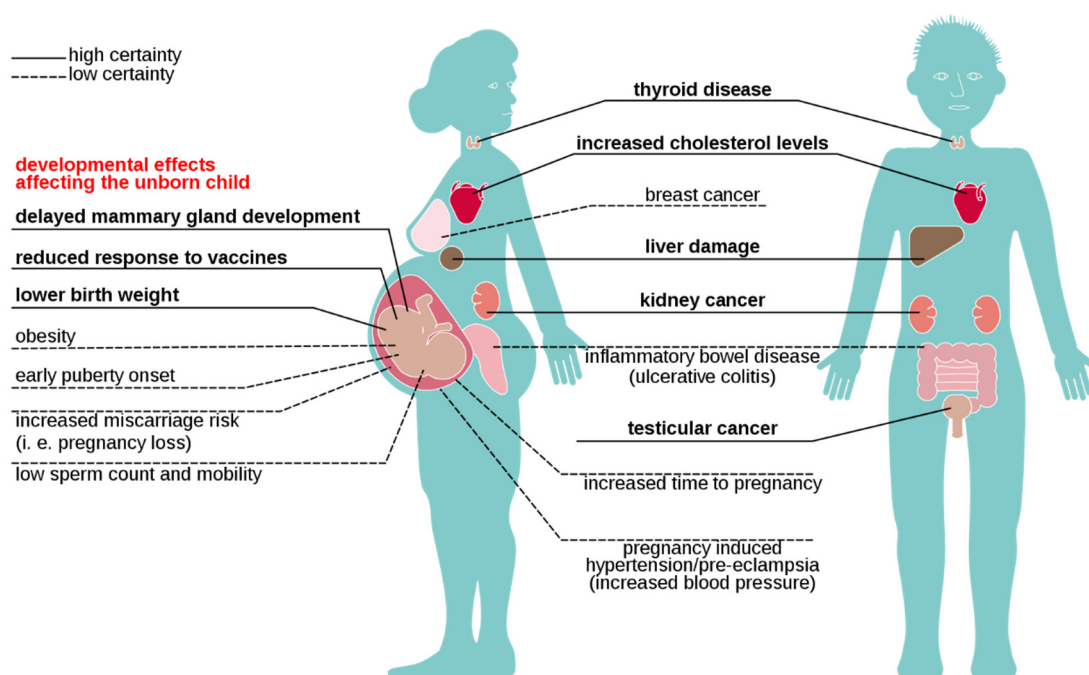


Figure 1. Effects of exposure to PFASs on human health. Some have confirmed certainty (continuous line), while others are still under study (dotted line) [17–22]. (From: <https://www.eea.europa.eu/publications/emerging-chemical-risks-in-europe/emerging-chemical-risks-in-europe> (accessed on 31 March 2021)).

PFOA and PFOS are long-chain acids, meaning that the fluoroalkyl moiety $(-CF_2)_n$ with $n \geq 6$ presents a higher potential for adsorption than short-chain ones, leading to greater bioaccumulation and hence toxicity [3,5]. The serum half-life of perfluorobutanesulfonic acid (PFBS) ($n = 4$) was found to be approximately 44 days, whereas for PFOA it was reported to be 21 months, and for PFOS 35 months. Consequently, the persistence of such compounds leads to increased damage to human health [6]. Moreover, the half-lives of PFOS and PFOA has been compared with those of other substances under different follow-up times, and the results evidenced that the elimination levels for PFOA were slower after the range of 12 and 24 months, meaning that the average half-life can be as long as 48 months [6]. In addition, PFOA strongly bioaccumulates in the environment as compared to PFBS, with partition coefficient

logarithms of 4.59 and 2.73, respectively [23]. Given the chemical structure of PFOA and PFBS, chains presenting the $(-CF_2)_n$ monomers with $n \leq 5$ are identified to be “safer” than longer chains. Further investigations are needed to better understand the behavior of short PFASs compounds and their effects on health.

A threshold of tolerable weekly intake (TWI) of 4.4 nanograms per kilogram of body weight per week is part of a scientific opinion on the risks to people’s health deriving from the presence of these substances in food [24]. However, in contaminated drinking water, PFASs are sufficiently “abundant” that the TWI is easily overpassed just by drinking 2 L of water per day since the monitoring system of many PWSs (Public Water Systems) already report concentrations far above the actual limit of 0.5 $\mu\text{g/L}$ of PFAS [3,25].

2.3. Physical Separation vs. Advanced Oxidation Processes

Physical separation methods remain the most common treatments for PFAS-contaminated liquids. Although such methods do not degrade PFAS, these processes are considered as a rapid solution involving only the mass transfer of PFAS from one media to another. These approaches can process extremely large volumes of liquid possessing low PFAS concentrations (levels of ppt to ppb), with the drawback of demanding consequent disposal, generally by incineration in furnaces [26].

Among physical separation technologies, the most employed techniques are procedures such as sorption on granulars of different particles, nanotubes of activated carbon (AC), biomaterials, molecularly imprinted polymers (resins), and mineral composites (e.g., zeolites). As mentioned, all these processes require further, generally off-site, treatment steps [27].

In the case of AC, the main issues are related to the poor removal of short-chained PFAS, difficulties in disposal, and eventually in the reactivation of carbon and the corresponding need for regeneration. These steps are necessary due to the reduction in removal efficiency with use. If frequent replacement of the material is ensured, AC can achieve 10–97% removal of PFAS [28].

The application of ion exchange resins provides up to 90–99% efficiency for some PFASs, although poor removal for selected PFAS is an unsolved problem, along with the potential complications related to the incineration and disposal of the adsorbents [29].

High-pressure filtration membranes are generally related to elevated capital and operation costs, uncertain corrosion control, lack of options for concentrate stream treatment or disposal, and finally membrane fouling. Furthermore, in this case, despite several disadvantages such as those mentioned above, the reported levels of PFAS removal from water range between 93% and 99% [30].

Emerging treatment methods are based on a series of chemical reactions which eventually result in PFAS degradation directly in water streams. Among these techniques, electrochemical oxidation, photocatalysis, photolysis, reduction processes using for example customized iodide or dithionite and sulfites, high-voltage electric discharges, bioremediation using microbial and fungal treatment, sonochemical degradation, ozonation under alkaline conditions, permanganate oxidation, sub or supercritical treatment, and microwave-hydrothermal treatments have been applied to PFAS degradation, with varying degrees of effectiveness [31]. Electrochemical oxidation, plasma, sonolysis, and hydrothermal/supercritical oxidation are some emerging technologies that are in the process of transitioning from laboratory-scale research to field-scale testing [32]. While promising, these technologies need extreme operating conditions, centralized laboratory equipment, and/or high chemical and energy requirements [30].

A combination of different approaches (perhaps using in situ and ex situ approaches) may be needed at a given site to cost-effectively address other areas with different water settings, orders of magnitude in concentration, co-contaminants, and remedial objectives. Selecting the most appropriate remedial strategy for PFAS is challenging. In this review paper we indicate the most promising technologies.

2.4. Analytical Techniques for PFAS Detection in Water

Qualitative and quantitative analysis of PFAS in water systems is extremely important, not only to assess the scale of contamination but also to inform and direct the development of remediation methods. Recent discussions [33] in the field of PFAS analysis highlighted the need to reach a consensus on standard methods for several analytes (short-chain PFAS in particular) and to validate methodologies beyond those for potable water. These objectives will require efforts regarding multi-laboratory validation for analytical methods.

Indeed, numerous analytical techniques for PFAS have been developed over time, in line with the observation of emerging contamination [33]. The most used methods in water systems to date are presented here.

2.4.1. Chromatographic Techniques

Several chromatography analysis techniques have been reported since the early 2000s, including gas chromatography (GC), high-performance liquid chromatography (HPLC), ultra-high-performance liquid chromatography (UHPLC), and capillary liquid chromatography (CLC). HPLC is in regular use for ionic PFASs such as perfluorinated carboxylic acids (PFCAs) and perfluorinated sulfonic acids (PFSAs), while GC is mostly employed for more volatile compounds such as fluorotelomer alcohols and perfluorinated sulfonamide ethanols [34]. Capillary electrophoresis has been investigated as an alternative for ionic and polar PFAS determination, but sensitivities and detection limits are lower than those of HPLC [31]. Specifically, the required detection limits for aqueous matrices can be in the range of parts-per-billion or even parts-per-trillion due to the health risks associated. For example, an analysis of groundwater contamination by recently identified PFAS compounds was conducted with a large-volume injection high-performance liquid chromatography (LVI-HPLC) procedure with a detection range of 0.71–67 ng/L (ppt) [35].

PFAS precursors varying in chain length (short or ultra-short chain) and moieties (anionic, cationic, or zwitterionic), have been detected in both tap and bottled water [36]. For ultra-short-chain PFAS, methods coupling LC to a quadrupole time-of-flight mass spectrometer (MS) as well as ultra-performance (UP) convergence chromatography coupled to MS were also reported [37,38]. The detection of 11 PFCAs and 4 PFSAs and short-chain PFCAs (C2–C8) at levels ranging from 70 to 200 ng/L in surface and ground waters was performed using HPLC-MS/MS [39,40], and an analysis of 19 PFAS in potable water was performed using UPLC-MS/MS [41].

HPLC coupled to ultra-high resolution orbitrap mass spectrometry (HPLC-uHRMS) for PFAS (C5–C17) monitoring showed to be advantageous in longer chain monitoring, with detection limits estimated at 0.005–0.2 ng/mL [42].

2.4.2. Sensing Systems for PFAS Detection

Since 2010, nanoscale materials have emerged as possible approaches for the monitoring of PFAS contaminants. Sensing nanomaterials present advantages due to the possibility of exploiting the unique physico-chemical properties of the nanometric size, such as aggregation, disaggregation, adsorption and desorption, potentially unparalleled sensitivity, and tunability. For example, chitosan-coated magnetite nanoparticles (Fe₃O₄-C18-chitosan-MNPs) were employed for the extraction of several PFAS compounds from both rainwater and tap water [43].

Gold nanoparticles (AuNP) are among the most studied nanosensors in general and for PFAS sensing. A significant improvement in this kind of sensing platform was obtained by employing peroxisome proliferator-activated receptor α (PPAR α)-responsive elements (PPRE) to modify AuNP sensors for the qualitative and quantitative analysis of PFAS in freshwater. This method was capable of detection at the ppt (2.5 ng/L) level [44]. Further efforts employing AuNPs were also reported using thiol-terminated-polystyrene,

polyethylene glycol and perfluorinated thiols, polydopamine-polyvinylidene fluoride membrane, and polydopamine [45–47].

The high sensitivity offered by surface-enhanced Raman scattering (SERS) was exploited to detect fluorosurfactants (FS) in groundwater using silver nanoparticles (AgNPs) for Raman enhancement. Immiscible ion pairs were formed between cationic dyes (methylene blue or ethyl violet) and anionic FSs. In addition, graphene oxide (GO) was used to enhance the loading of FSs [48].

2.4.3. Total Fluorine Analysis (TF)

Typical methods for organic and inorganic TF determination include particle-induced gamma-ray emission (PIGE), absorbable organic fluorine (AOF), and combustion ion chromatography (CIC). Recently, fluorine-19 nuclear magnetic resonance spectroscopy (^{19}F -NMR), inductively coupled plasma-mass spectrometry (ICP-MS/MS), and X-ray photoelectron spectroscopy (XPS) were also reported on for fluorine detection [49–51].

3. Advanced Oxidation Processes (AOPs) for PFAS

3.1. Heterogeneous Photocatalysis Materials

Heterogeneous photocatalysis involving semiconductor catalysts provides one of the best remediation techniques for PFAS remediation by involving UV-Vis light and sometimes oxidation reactants [52–55]. The most important advantage of using photocatalysis is that both photo-oxidation and photoreduction pathways operate in tandem to effectively decompose PFAS to shorter-chain perfluoro carboxylic acid (PFCA) by the stepwise elimination of CF_2 groups. Finally, these PFCA intermediates completely mineralize to CO_2 and fluoride ions through repeating similar steps. The photocatalytic material, along with appropriate opto-electronic features, must also be chemically stable, recyclable, non-toxic, and available with a low price tag. Based on these requirements, Ti, Ga, In, and Bi-based compound photocatalysts have been primarily implemented in the literature to remove PFAS from wastewater (Table 1).

3.1.1. Metal Oxides

TiO_2 was the first photocatalyst investigated for the removal of PFOA in water bodies [56] due to its well-known high activity towards the degradation of pollutants. However, TiO_2 showed a very low reaction rate constant ($\sim 0.0001 \text{ min}^{-1}$), and high half-life ($\sim 6931 \text{ min}$) for PFOA degradation [57]. Similar problems were observed in the presence of titanate nanotubes (TNTs) synthesized by hydrothermal methods to improve the surface area, which were even less effective in removing PFAS under UV light [58]. This inefficiency of Ti-based photocatalysts was attributed to the strong repulsion of anionic PFAS molecules from the negatively charged surface of TNT. Commercial P25 TiO_2 , a benchmark in the field, was able to complete the degradation reaction of PFOA within 4 h under illumination with 254 nm UV light [59]. However, under higher wavelength light (315–400 nm), the degradation of PFOA decreased drastically. The photocatalytic ability of TiO_2 to degrade organic pollutants mainly relies on the formation of HO^\bullet and O_2^\bullet radicals by oxidation of water and reduction of O_2 through photogenerated holes and electrons, respectively. Nevertheless, both these reactive oxidation species (ROS) are less active for the decomposition of PFOA. Thus, in the case of TiO_2 , photogenerated h^+ and e^- directly initiate the decarboxylation of PFAS to mineralize them to CO_2 and fluoride ions in a stepwise manner. For this phenomenon to occur, the absorption of PFAS molecule on TiO_2 surface becomes a necessary condition. This can be achieved by spreading positive surface charges on the TiO_2 by carrying out the photocatalytic reaction of PFAS in acidic conditions. Panchangan et al. [56] showed that in the presence of 0.15 M perchloric acid, the rate constant of PFOA degradation increased by ~ 46 times with respect to that performed in the absence of acid. Following this work, most of the research for TiO_2 -based

photocatalytic degradation of PFAS was performed at a pH below 4. Acids such as oxalic acid increase the photoreduction capability of TiO₂ to degrade PFAS. Wang et al. [60] demonstrated that adding oxalic acid leads to the formation of carboxyl anion radicals (CO₂^{-•}) by photogenerated holes that have a higher reduction potential (−1.85 V) than that of photogenerated electrons. The same work also reported that oxalic acid is ~11.6 times more effective in PFOA decomposition than perchloric acid under the equivalent pH of the reaction. TiO₂ nanoparticles in the presence of oxalic acid effectively degrade 86.7% of PFOA in 180 min under N₂ bubbling.

TiO₂ supported on carbon allotropes such as MWCNT [61], graphene [62], and reduced-graphene oxide (rGO) [63] also increased the direct interaction between PFOA and TiO₂ photocatalysis owing to the high adsorption capacity of the carbon-based material provided by the high surface area and surface functional group. Carbon can also trap the photogenerated electrons of TiO₂ and reduce the electron–hole recombination process during the photocatalytic reaction. TiO₂-MWCNT and TiO₂-rGO were able to degrade ~100% of PFOA under UV irradiation in 8 h and 12 h, respectively. Recently, Shen et al. [64] fabricated TiO₂ quantum dots of 2–5 nm in size on sulfonated graphene nanosheets using sodium dodecyl sulfate as a surfactant (Figure 2a). Due to the hydrophobic nature of sulfonate graphene and highly dispersed TiO₂ quantum dots, PFOA pollutants could instantaneously be adsorbed on the surface, followed by fast decomposition by eliminating CF₂ species. Apart from carbon, molecule-imprinted polymer (MIS)-modified TiO₂ nanotubes also boosted contact between PFOA and TiO₂ and reduced the recombination of h⁺ and e⁻ pairs by capturing photogenerated electrons [65].

Noble metal nanoparticles deposited on TiO₂ can also act as an electron sink to increase the lifetime of photogenerated h⁺ and e⁻ pairs. Among Pt, Pd, and Ag nanoparticles deposited by TiO₂, Pt-TiO₂ showed a considerable improvement (~12.5 times) in the photocatalytic performance of PFOA removal as compared to pure TiO₂ [66]. With the highest work function, Pt can attract more electrons from TiO₂ to form a strong Schottky barrier at the interface, which improves h⁺/e⁻ separation during irradiation. Weon et al. [67] successfully loaded Pt nanoparticles on the reductive sites of the TiO₂ facet to precisely capture photoinduced electrons (Figure 2b). This charge separation led to an increase in the number of holes on TiO₂ sites which participate in PFOA degradation. At the same time, electrons on the Pt atom produced hydrogen atoms and led to hydrogen spillover onto the TiO₂ surface. The Ti-H bond formed on the surface facilitates hydrodefluorination of PFOA through the cleavage of the C-F bond. In addition to reducing recombination, doping with transition metals like Cu, Fe, and Pb also increased visible light absorption by lowering the band gap of TiO₂, leading to superior photocatalytic degradation of PFAS [57,68]. Combining different strategies can lead to significant advancements in photocatalytic performance by creating a synergetic effect. Fe-deposited titanate nanotubes (TNT) supported on activated carbon (AC) (Fe/TNTs@AC) demonstrated highly efficient photodegradation of PFOA (~90%) in 4 h under UV light irradiation with 62% of the defluorination reaction [69]. In Fe/TNTs@AC, the nanotube architecture and AC provided a high surface area, while α-Fe₂O₃ particles and AC considerably boosted PFOA adsorption on the surface and separation of the h⁺/e⁻ pair by acting as the electron acceptor. Fe/TNTs@AC was recycled without significant loss in adsorption and degradation capacity of the photocatalyst. Similarly, Ga/TNTs@AC showed faster adsorption kinetics and degraded ~75.0% while mineralizing 66.2% of PFOS after 4 h of UV irradiation [70]. This type of study opens an avenue towards developing more such TiO₂-based photocatalysts by integrating different strategies, with each modification step playing a specific role.

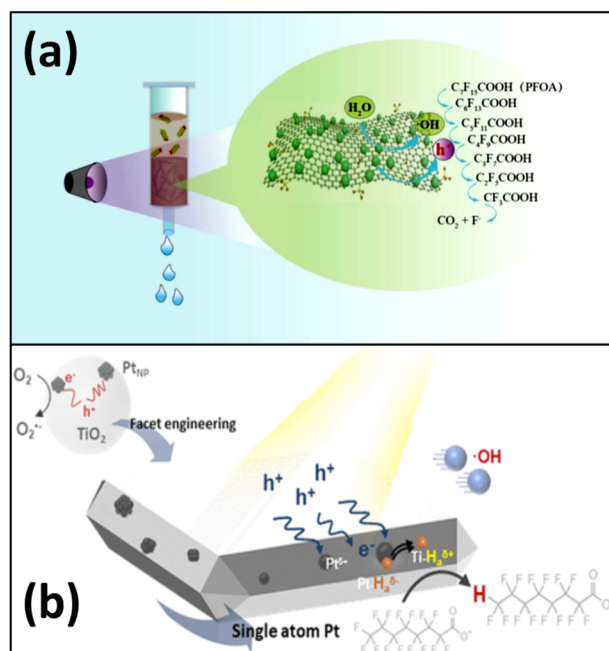


Figure 2. PFOA degradation using (a) TiO₂ quantum dots supported on sulfonated graphene nanosheets (reprinted from [64], copyright (2020) with permission from Elsevier) and (b) single Pt atoms loaded on the reductive sites of the TiO₂ facet (reprinted from [67], copyright (2021) with permission from ACS Publications).

Along with TiO₂, ZnO was also studied for remediating wastewater from PFAS but with limited success [71]. Although heterojunction between ZnO/rGO did degrade 90.9% of PFOA [72], no other work on ZnO has been reported.

With a more negative conduction band edge and a wider band gap (4.8 eV) than TiO₂, gallium oxide (Ga₂O₃) displayed a better capability for removing PFAS than TiO₂. In contrast to TiO₂, the scavenging experiment proved that the breaking down of PFOA proceeds via a reduction reaction in Ga₂O₃ involving photogenerated electrons to produce a rate constant ~19 times higher than that of TiO₂ [73]. Nanostructured Ga₂O₃ in nanoneedle [74], sheaf-like [75], and nanorod [76] forms with improved surface area presented escalation in the demolition of PFOA from wastewater. Among them, the sheaf-like nanostructure assembled with nanoplates of an average width of 100 nm and thickness of 10 nm exhibited the highest reaction rate constant (4.85 h⁻¹). Compared to commercial Ga₂O₃ and TiO₂ powder, this value was ~16 and ~44 times higher, respectively. Nevertheless, the mechanism involved in all the nanostructures remained same where photoinduced electrons were used for the decarbonization of PFOA followed by HF elimination. To improve photocatalytic activity towards PFOA degradation, Huang and coworkers [77] modified Ga₂O₃ hierarchical nanosheets by doping a series of transition metals (Mn, Co, Zn, Cu, Ti, and In). Indium doping in the Ga₂O₃ hierarchical composite resulted best, completely degrading PFOA within 1 h with degradation kinetics ~7.8 times higher than those of pristine Ga₂O₃ (Figure 3a).

By investigating the reaction mechanism, this considerable improvement was attributed to not only enhanced light absorption and charge separation but also to the activated surface that provided conducive conditions for better adsorption of PFOA.

In₂O₃ is highly active in removing PFAS, and it follows a similar photo-oxidation pathway as TiO₂, but with significantly higher photocatalytic performance with a reaction rate approximately ~59 times higher than that of TiO₂ [10]. As In₂O₃ provides the surface with better adsorption capacity for PFOA, photogenerated holes directly attack the carboxyl group of PFOA rather than forming the HO· radical as in TiO₂. Since the surface plays the prime role in In₂O₃, substantial work on In₂O₃ was dedicated to refining the surface area by fabricating different nano morphologies like nanospheres, nanoplates,

photocatalytic reactions. Most importantly, the formation energy for oxygen vacancies (OVs) of BiOX is very low, generating an abundant quantity of OVs on the surface. This feature further modulates the bandgap, providing sites for electron capture to delay the recombination of photogenerated charge carriers. The oxygen-deficient sites further participate in binding PFAS pollutants, with optimum interactions as compared to metal oxide. The layered structure of BiOX also offers a large surface-to-volume ratio with extensive exposure of active facets like (001). Because of these merits, BiOX showed an exceptional capability towards the photodegradation of PFOA, as reported first by Song et al. [87] for BiOCl. In their subsequent work [88], the same group systematically performed experiments to prove the linear relationship between the OVs and the photodegradation of PFOA. Doubling the OVs in BiOCl led to a four-fold increase in efficiency of defluorination in PFOA. The wide-bandgap BiOF photocatalyst can be modified by inducing OVs, which introduce the intermediate band in the forbidden gap to lower the energy required to excite the electrons by irradiation [89]. A study conducted by Zu and coworkers [89] demonstrated that OVs could be tuned on exposed (001) facets of BiOF by adjusting the concentration of ethylene glycol during synthesis. The BiOF (001) produced by using 50% ethylene glycol could completely decompose PFOA within 6 h based on developed OVs. BiOI material, even with the smallest bandgap of ~1.8 eV, was not conducive to the photocatalytic removal of PFAS, mainly owing to the lower valence band edge than that of the redox potential of (HO^-/HO^\bullet) [90]. However, BiOI_{0.95}Br_{0.05} displayed considerably high photocatalytic activity, requiring only 2 h to decompose 96% and 3 h to mineralize 65% of PFOA, thus showing the significance of the small amount of Br doping [90]. Here, rather than ROS, the holes and electrons played a more dominant role in the photocatalytic process. Doping of Br led to a reduction in bandgap for enhanced light harvesting and increased exposure of the (001) facet to elevate the separation of h^+/e^- pairs. This promoting characteristic of BiOI_{0.95}Br_{0.05} produced a degradation rate constant ~4.3 times higher than that of BiOI. A similar boost in photocatalytic performance was observed when BiOI was mixed with BiOF and loaded with Bi nanoparticles to provide Bi/BiOI_{1-x}F_x [91]. Integrating both these bismuth oxyhalides further reduced the bandgap to increase the visible light absorption and elevated the surface area by two times due to the formation of hollow flower-like microspheres. On the other hand, Bi nanoparticles on the surface give rise to a surface plasma resonance effect to favor photogenerated charge separation by generating an electric field near the junction. Because of these properties, the Bi/BiOI_{0.8}F_{0.2} composite presented the best activity for the decomposition of PFOA (40 mg/L) in just 2 h of illumination of simulated solar light with a ~10 times higher degradation rate than that of pure BiOF and BiOI. As per the results of the EPR spectra and scavenging experiment, superoxide radicals ($O_2^{\bullet-}$) are dominant species for dissociating the bonds of PFOA. The p-n heterojunction of BiOI@Bi₅O₇I (Figure 4a) was formed to improve charge separation by the facile heat treatment of BiOI in the air at a moderate temperature of 390 °C [92].

The resulting p-n heterojunction causes photogenerated electrons to be immediately driven to the conduction band of Bi₅O₇I while leaving the holes in the valence band of BiOI, thereby spatially separating h^+/e^- pair. This heterojunction is efficient in degrading 80% of PFOA in 6 h under irradiation with visible light, with the HO^\bullet radical as the oxidizing agent. Similar charge separation was observed in the case of the Bi₅O₇I/ZnO n-n heterojunction microsphere, but here photogenerated holes were found to be responsible for attacking carboxylic groups of PFOA [93].

A novel Bi₃O(OH)(PO₄)₂ (BOHP) compound, despite having a larger bandgap and lower surface area than BiPO₄ and β -Ga₂O₃, showed ~15 times higher photocatalytic activity towards the degradation of PFOA [94]. The highly positive surface charge of BOHP induces an incremental rise in the adsorption behavior of PFOA on the surface. Along with this, the favorable redox potential of the BOHP also participates in enhancing PFOA mineralization. The performance of BOHP was amplified by Xu et al. [95], forming composites with carbon spheres (CS) and upgrading the stability of BOHP by suppressing

the photo corrosion of the composites via acting as an electron sink. The adsorption capacity of PFOA was also improved through CS, which contributes to the adsorption of PFOA. Carbon spheres were also found to be beneficial for an iron (hydro)oxide photocatalyst (FeO), where a 1:1 composite of FeO/CS was developed by the same research group that presented the BOHP/CS composites (Figure 4b) [96]. Here, CS aids in forming ferrihydrite on the surface, which improves the adsorption of PFOA via binuclear and bidentate complexation and increases direct electron extraction from PFOA under stimulated solar light. FeO/CS was able to photodegrade 95.2% of PFOA, with 57.2% defluorination in 4 h in neutral pH.

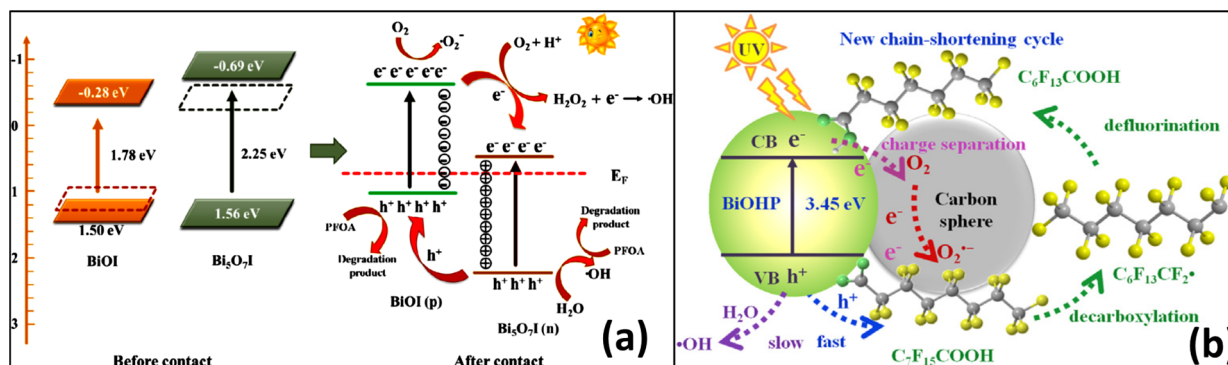


Figure 4. Charge separation and PFOA degradation (a) at the p-n heterojunction of BiOI@Bi₅O₇I (reprinted from [92], copyright (2020) with permission from Elsevier) and (b) in BOHP/CS composites (reprinted from [95], copyright (2020) with permission from Elsevier).

The wide-bandgap semiconductor boron nitride (BN) was also reported for photocatalytic degradation of PFOA under UV light (Figure 5a) [97]. Boron nitride followed a similar photo-oxidation pathway as TiO₂, mainly involving holes to bifurcate PFOA but with rate twice that of TiO₂. The exfoliation of BN layers through ball milling further improved the degradation rate. Tungstic heteropoly acid (H₃PW₁₂O₄₀) supported on high-surface-area bimodal mesoporous silica (BMS) displayed an enhanced defluorination rate of PFOA compared to direct photolysis under vacuum UV light irradiation with a wavelength of 185 nm [98]. Recently, a Z-scheme-based heterojunction was discovered to be highly effective in photocatalytic applications, considering its ability to cause charge separation at the junction to increase the lifetime of photogenerated charges. Tang et al. [99] fabricated a Z-scheme heterojunction of core-shell CeO₂@NiAl-LDHs (Figure 5b) to proficiently remove PFOA from wastewater. A built-in electric field in the Z-scheme heterojunction causes instantaneous separation of photogenerated charges to record photodegradation of 90.2% of PFOA under stimulated solar light. Although implementing various photocatalytic materials and their different forms and compounds provides the solution for adequate removal of PFAS, maintaining a conducive environment during the photocatalytic reaction is equally vital. Factors such as aerobic or anaerobic conditions, type of light used, pH and temperature of the solution, and the presence of other impurities are crucial in deciding the photocatalytic degradation rate of PFAS. The effect of these factors is covered in other review articles [100–103], and is out of scope for the present report.

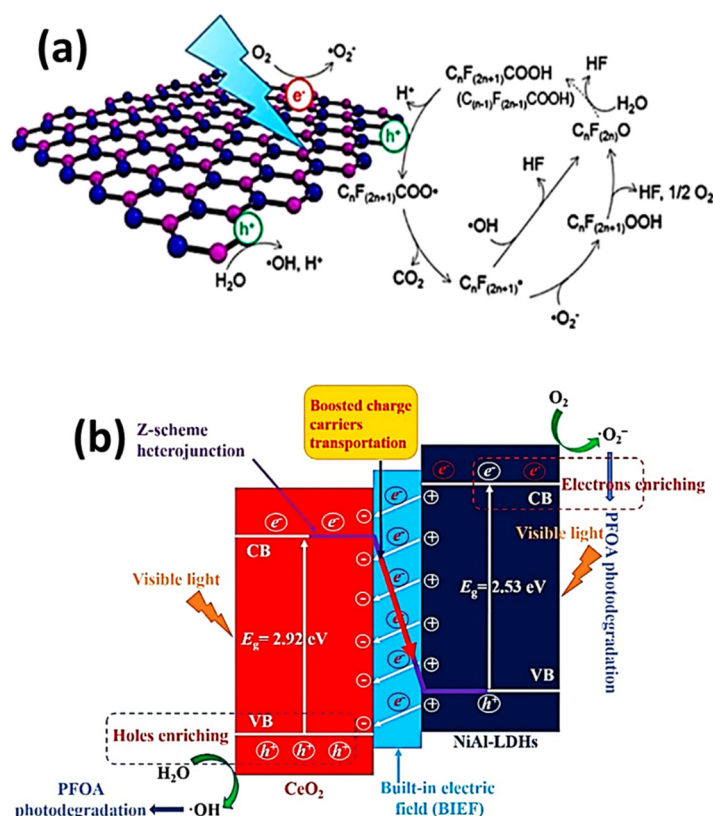


Figure 5. PFOA degradation mechanism over (a) boron nitride (reprinted from [97], copyright (2020) with permission from ACS publications) and (b) the z-scheme based heterojunction of core-shell $\text{CeO}_2@$ NiAl-LDHs (reprinted from [99], copyright (2021) with permission from Elsevier).

Table 1. Heterogeneous photocatalysis applied to PFAS decontamination.

Photocatalyst	Photocatalytic Performance				Photocatalytic Reaction Condition				Ref
	Reaction Time (h)	Rate Constant (min^{-1})	% Degradation	% Defluorination	Concentration of PFOA/PFOS	Catalyst Dosage (g/L)	pH of Solution	Light Source	
TiO_2	12	0.0001	15%	---	50 mg/L	0.5	5	254 nm and 400 W	[57]
Titanate nanotubes	24	---	59%	---	120.8 μM	0.125	4	254 nm and 400 W	[58]
P25 TiO_2	3	0.0005	30%	----	12 mM	0.66	3	310–400 nm and 75 W/m ²	[59]
$\text{TiO}_2\text{-HClO}_4$	7	0.0047	97%	38%	120 μM	0.66	2.47	254 nm and 16 W	[56]
$\text{TiO}_2\text{-Oxalic acid}$	3	---	86.7%	16.5%	24 μM	0.5	2.47	254 nm and 23 W	[60]
$\text{TiO}_2\text{-MWCNT}$	8	---	100%	----	72.5 μM	0.4	5	365 nm and 300 W	[61]
$\text{TiO}_2\text{-rGO}$	12	0.0027	93 \pm 7%	20%	240 μM	0.1	3.8	254 nm and 150 W	[63]
$\text{TiO}_2\text{-MIP}$	10	0.0044	81%	30.2%	72.5 μM	--	5	254 nm and 23 W	[65]

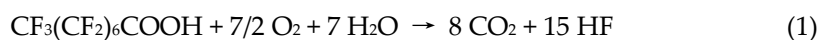
TiO ₂ QD/Graphene	10	0.0098	~90%	----	300 µM	0.02	5	UV light 150 W	[64]
TiO ₂ -Pt		0.0121	100	34.8					
TiO ₂ -Pd	7	0.0073	94.2	25.9	144.9 µM	0.5	3	365 nm and 135 W	[66]
TiO ₂ -Ag		0.0021	57.7	8.1					
TiO ₂ -Cu	12	0.0031	91	19					
TiO ₂ -Fe	4	0.0015	60	--	121 µM	0.5	5	254 nm and 400 W	[57]
TiO ₂ -Pb	4.5	0.0086	99	22.4	121 µM	0.5	5	254 nm and 400 W	[68]
TiO ₂ -Pt single atom	2		40	35	100 µM	0.25	7	254 nm and 7.87 mW/cm ²	[67]
Fe/TNT@AC	4	0.0153	90	62	100 µM	1	7	254 nm and 21 mW/cm ²	[69]
Ga/TNT@AC	4		75	66.2	0.1 mg/L	3	7	254 nm and 210 W/m ²	[70]
ZnO	3 days	---	95	---	25.5 µM	1	6.5–7.0	365 nm and 13 W/m ²	[71]
Ga ₂ O ₃	3	0.0020	36	15	0.5 mg/L	0.5	--	254 nm and 14 W	[73]
Ga ₂ O ₃ needle-like	40 min	0.0380	100	58	0.5 mg/L	0.5	--	254 nm and 14 W	[74]
Ga ₂ O ₃ sheaf-like	45 min	0.0240	100	60	0.5 mg/L	0.5	---	254 nm and 14 W	[75]
β-Ga ₂ O ₃ nanorods	1.5	0.0425	98.8	56.2	10 mg/L	0.5	3	254 nm and 50 W	[76]
In-doped Ga ₂ O ₃ nanosheets	1	0.0416	100	--	20 mg/L	0.5	--	Hg lamp	[77]
In ₂ O ₃	4	0.006	75	33	40 mg/L	3.4	5	254 nm and 23 W	[10]
In ₂ O ₃ microspheres	17 min	0.130	100	--				254 nm	
In ₂ O ₃ nanocubes	2	0.030	100	--	30 mg/L	0.5	3	and 15 W	[78]
In ₂ O ₃ nanoplates	42 min	0.073	100	--					
In ₂ O ₃ nanoporous nanospheres	30 min	0.100	100	71	30 mg/L	0.5	3.9	254 nm and 23 W	[9]
In ₂ O ₃ porous nanoplates	30 min	0.158	100	---	30 mg/L	0.5	---	254 nm and 15 W	[79]

MOF-derived In ₂ O ₃ nanospheres	3	---	100	50	10 mg/L	0.2	---	254 nm and 32 W	[80]
In ₂ O ₃ /graphene	3	0.008	100	60.9	30 mg/L	0.5	3	254 nm and 15 W	[81]
In ₂ O ₃ /Ce ₂ O ₃	1	0.063	100	53.3	100 mg/L	0.4	--	254 nm and 500 W Xenon	[82]
In ₂ O ₃ /MnO _x	3	0.301	100	17.4	50 mg/L	0.5	3.8	lamp and 500 W 254 nm	[83]
InOOH	3	0.008	83.4	---	20 mg/L	0.25		and 18 W 254 nm	[84]
BiOCl	12	---	100	59.3	20 µM	0.5	4.8	and 10 W Xenon	[87]
BiOCl with OV	8.5	---	68.8	12.86	50 µM	1	2	lamp and 300 W	[88]
BiOF	6	0.006	100	56.8	15 mg/L		3–5	UV light	[89]
BiOI	2	0.0048	66	37% in 3h	20 mg/L	0.4	--	Hg lamp and 300 W	[90]
BiOI _{0.95} Br _{0.05}	2	0.0205	100	65% in 3h	20 mg/L	0.4	--	Hg lamp and 300 W Xenon	[90]
Bi/BiOI _{1-x} F _x	2	0.0375	100	10	40 mg/L	0.4	3–5	lamp and 800 W Xenon	[91]
BiOI@Bi ₅ O ₇ I	6	0.0041	81	60	15 mg/L	0.5	3	lamp and 800 W Xenon	[92]
BiOI/ZnO	6	0.0002	91	52.2	1 mg/L	0.5	4	lamp and 500 W 254 nm	[93]
BOHP	1	0.1000	100	60	0.13 mM	1.8	4	and 18 W 254 nm	[94]
BOHP/CS	4	---	100	32.5	0.2 mg/L	1.0	7	and 18 W	[95]
FeO/CS	1	---	95.2	57.2	0.2 mg/L	1.0	7	Stimulate d solar light 254 nm	[96]
Boron nitride	4		100	52	0.12 mM	2.5	6.5	and	[97]

H ₃ PW ₁₂ O ₄₀ /bimodal mesoporous silica	4	0.0018	50	10 mg/L	0.2	4	24 W 254 nm and 8 W	[98]
--	---	--------	----	---------	-----	---	------------------------------	------

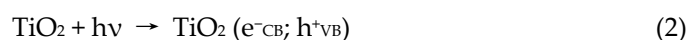
3.1.3. Reaction Mechanisms

The mineralization of PFOA in water can be summarized as in Equation (1)

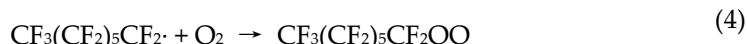


The reaction has been investigated in irradiated aqueous suspensions of TiO₂, one of the most extensively investigated photocatalysts, and the commonly accepted mechanism is the result of a photo-redox and β-scission pathway [104]

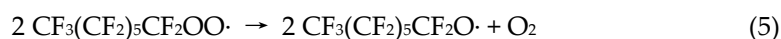
Upon irradiation of suitable energy, electrons (e⁻_{CB}) and holes (h⁺_{VB}) are localized respectively within the conduction and valence band of TiO₂ [105], according to Equation (2).



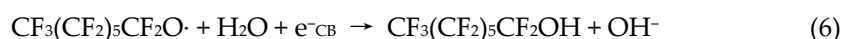
It is worth noting that PFOA exists mainly in its deprotonated form under natural pH conditions. Deprotonated PFOA undergoes hole-induced Kolbe decarboxylation [60,106,107], giving rise to the C7 radical intermediate (Equation (3)), which in turn reacts with molecular oxygen, producing a peroxy-radical [108] (Equation (4))



The coupling of two peroxyradicals forms molecular oxygen and two oxyradicals (Equation (5)).



The oxyradical undergoes electron-coupled hydrogen abstraction from water and evolves to an unstable primary perfluorinated alcohol [109] (Equation (6)), which eventually leads to acylfluoride and hydrogen fluoride [110] (Equation (7))

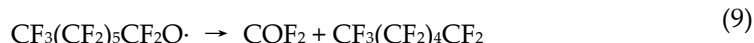


Finally, the acyl fluoride undergoes hydrolysis to the C6 carboxylic acid (Equation (8))



This in turn can undergo the same photo-redox mechanism several times until the chain length is reduced step by step [111].

Another pathway relies on the capability of the oxyradical C7 generated in Equation (5) to undergo monomolecular β-scission by eliminating fluorofosgene (COF₂) and giving rise to a C6 perfluoroalkyl radical [112–114] (Equation (9)).



Fluorofosgene is easily hydrolyzed to HF and CO₂ (Equation (10))



The perfluoroalkyl radical can undergo the reaction steps as described above, starting from Equation (4). The mechanism described above is schematically represented in Figure 6.

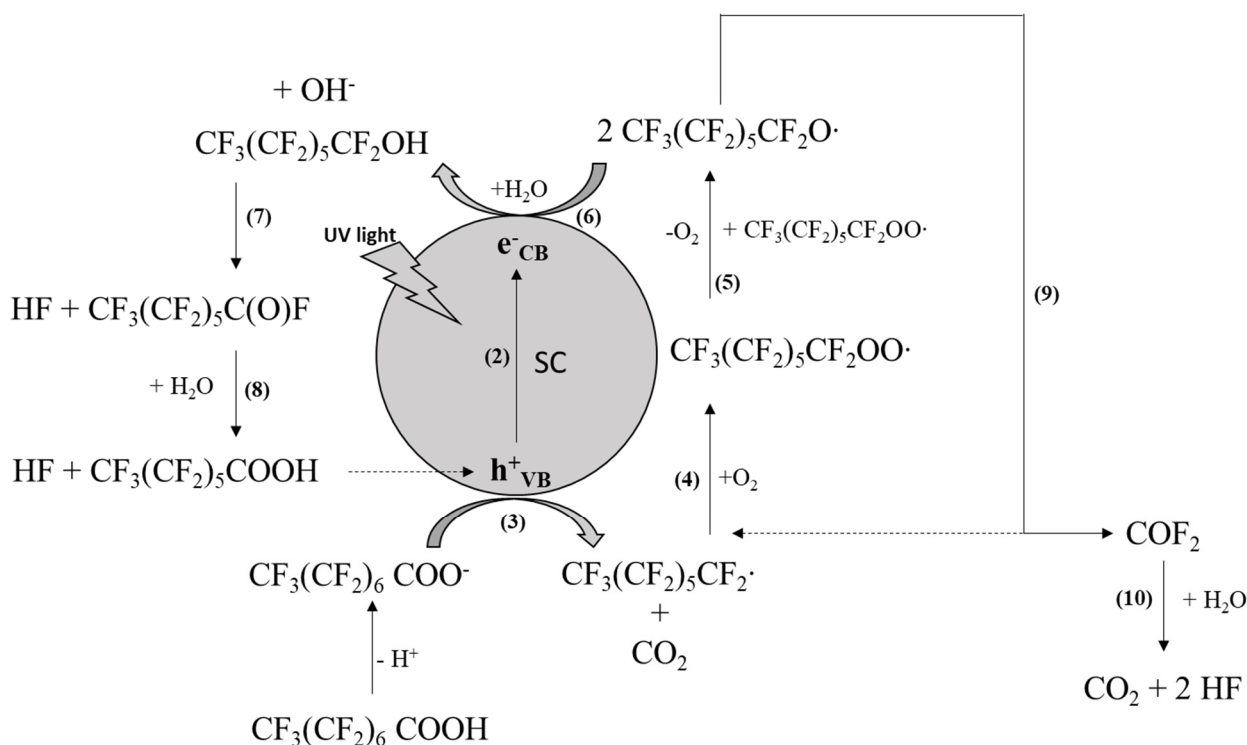
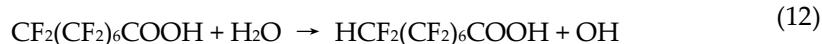


Figure 6. A hypothesized degradation mechanism of PFOA. Dashed lines indicate that the C_n product undergoes the same path, reducing the number of carbon atoms step by step.

Notably, the β -scission mechanism (Equations (9) and (10)) induces the decomposition of PFOA without forming carboxylic intermediates, which instead are produced when the photoredox mechanism (Equations (3)–(8)) occurs. Therefore, the concentration of shorter-chain perfluorinated acids should increase proportionally to fluoride formation if the photoredox mechanism preferentially occurs. Gatto et al. [104] observed that the shorter-chain carboxylic acids slowly started to form after switching on the lamp, but during the first hours of reaction, a direct correlation between PFOA mineralization and fluoride formation was evident. This suggests that the reaction takes place initially through the predominant β -scission mechanism, which efficiently competes with the photo-redox one. The authors also observed a slight loss of fluoride ions of ca. 3% in the aqueous phase, possibly due to fluorination of the surface of TiO₂.

On the other hand, for longer reaction times the mineralization of PFOA nearly stopped, and an enhanced formation of shorter chain carboxylic acids was observed, with a concentration trend following the molecular weight of the intermediates. This indicates the preferential occurrence of the photo-redox mechanism with longer reaction times.

Another mechanism proposed in literature relies on the initial one-electron reduction of PFOA by photogenerated electrons, which results in the defluorination of the terminal perfluorinated carbon atom and the consequent formation of the corresponding perfluoroalkyl radical (Equation (11)). The latter in turn abstracts a hydrogen atom from the water, forming an OH radical and a monohydrogenated intermediate (Equation (12)). Repeating the same pathway results in the progressive hydrogenation of the alkyl chain, eventually leading to mineralization [54].

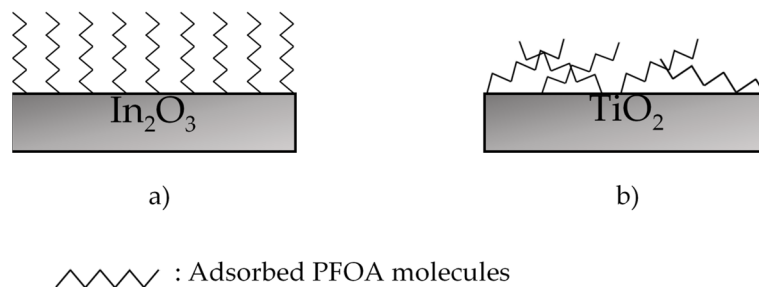


This pathway seems less probable compared to the other above-mentioned pathways considering the reduction of oxygen, which should preferentially occur.

Finally, it is worth noting that direct photolysis of PFOA could take place only under irradiation shorter than 220 nm, which corresponds to the bond dissociation energy of the C-F bond, i.e., ca. 544 kJ/mol [102,115].

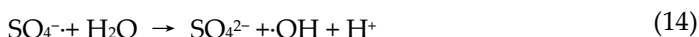
Only ca. 10% of degradation was observed through photolysis at 254 nm [116, 117].

It is worth noting that PFOA is almost inert towards the OH radicals produced in the presence of irradiated TiO₂ ($k_{\text{OH}+\text{PFOA}} \leq 10^5 \text{ M}^{-1} \text{ s}^{-1}$) [118], due to the absence of hydrogen atoms prone to OH radical abstraction in the PFOA structure. Moreover, the initial decarboxylation (Equation (3)) is not likely to be induced by OH radical attack. In fact, the perfluorination of the alkyl chain reduces the electronic density of the carboxylic moiety, making the OH radical-mediated electron transfer unfavorable. Therefore, TiO₂, generally very active for the degradation of a wide range of organic substrates, is rather poorly efficient in the degradation of PFOA. Its activity is slightly enhanced only under highly acidic pH conditions (HClO₄, pH < 2) [56, 119] where the pH-dependent potential of the photogenerated holes is higher. An analogous situation is observed for the TiO₂-induced degradation of trichloroacetate, which does not possess any hydrogen atoms [120]. Therefore, the lower the efficiency of hole-induced water oxidation to OH radicals, the better the efficacy obtained in terms of PFOA degradation. Accordingly, other semiconductors with a poor ability to produce OH radicals are instead more active in PFOA degradation. For instance, Li et al. [10] found that the apparent rate constant for the degradation of PFOA was 8.4 times higher in the presence of In₂O₃ than in the presence of TiO₂. This result was justified by considering the peculiar adsorption mode of PFOA onto the In₂O₃ surface and the higher hole availability for PFOA oxidation with respect to TiO₂, where water oxidation preferentially occurs. PFOA is bound to In₂O₃ in a bidentate or bridging configuration, resulting in a vertical and ordered arrangement of chains (Figure 7a). On the TiO₂ surface, PFOA instead binds in a monodentate way (Figure 7b) which results in a tilted configuration of the chains.



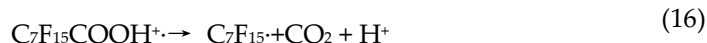
degradation rate 32.5 times higher with respect to the bare material [68]. Authors attributed the enhanced activity to the capability of Pb for acting as an electron trap, thus increasing the availability of holes for the degradation of PFOA.

Persulfate ($S_2O_8^{2-}$) has also been used as a promising alternative for the degradation of PFOA. The preliminary activation of persulfate is required to generate sulfate radicals (Equation (13)), which in turn may directly induce oxidation or react with water, producing OH radicals (Equation (14)) [123]. This reaction is slow at room temperature ($k = 2 \times 10^{-3} \text{ s}^{-1}$) but quickly proceeds at higher temperatures [124].



The activation of persulfate can be performed through thermal energy. For instance, complete defluorination of PFOA (0.1 mM) was observed after 18 h at 70 °C [125]. Several other methods to activate persulfate have been proposed to degrade PFAS, including ultraviolet, microwave, Fe^{2+} , and ultrasound approaches. However, the highest defluorination efficiency was achieved by heat activation [126].

Sulfate radicals induce PFOA degradation but with a much lower defluorination ratio, indicating an insufficient degree of mineralization. Several short-chain perfluoroalkyl carboxylates (C2-C6) have been identified [127, 128]. The proposed reaction mechanism proceeds with a sequential elimination of CF_2 groups [129]. Decarboxylation of PFOA is induced by sulfate radical attack through the formation of a radical cation intermediate (Equations (15) and (16)).



The resulting radical couples with an OH radical, producing the unstable alcohol intermediate which eventually evolves according to Equations (7)–(10).

4. Direct Photolysis

Given that PFAS does not absorb visible light and absorption is generally limited to the UVC region [130], the use of solar irradiation is not possible and artificial sources are required. In fact, the dissociation energy for C-F bonds can be up to 544 kJ/mol [102], corresponding to photons of 220 nm. UV light sources of wavelength < 220 nm and high power are somewhat less common than their UV-A or B counterparts. They have generally lower lifetime, require more specialized equipment and safety precautions, and as such the associated costs are higher. This is reflected by the scarcity of reports focusing on this approach present in literature. Nevertheless, important results can be found either in dedicated reports or extracted from photocatalysis papers where they appear as baseline or control experiments. Some results are collected in the Table 2 below:

Table 2. Direct photolysis of PFAS compounds in water.

Irradiation Wavelength (nm)	Power (Electrical, W)	Substrates	Reaction Time	Degradation/Defluorination Yield (%)	Ref.
254	200	PFOA 1.35 mM	72 h.	89/33	[116]
254	15	PFOA 0.025 mM	6 h.	13/2	[131]
185 (prevalent) 254 (prevalent)	20	PFOA 0.12–2.42 μ M	3 h.	87/21 31/0.5	[132]
185	15	PFOA 60 μ M	2 h.	62/17	[133]
220–460	200	perfluoropropionic acid, perfluorobutyric acid, perfluoropentanoic acid	24 h.	16–24/9–12	[134]
254	36	PFOA 0.024 mM	8 h.	20/9	[135]

254

24

PFOA 1 mg/L

24 h.

21/9

[136]

Although direct photolysis seems to be moderately effective for initiating degradation, the reported defluorination yields are quite low, indicating that complex mechanisms are taking place rather than simple photoinduced bond dissociation. Along with the problems related to equipment, the difficulties presented by the direct photolysis approach provide the motivation to investigate other methodologies, for example where light absorption is performed by a photocatalyst (as described in the previous section).

5. Methods Based on a Sacrificial Radical Source

A different approach involves the presence of a sacrificial agent in the solution, enabling pathways based on the generation of radical species. Among these latter, it is worth mentioning the use of aqueous electrons to perform reductive defluorination, as explored by Qu et al. [131]. These authors employed potassium iodide to generate hydrated electrons from a water-iodide complex under 254 nm wavelength irradiation from a 15 W lamp. A combination of photolysis and reduction by electrons then yielded a 96% defluorination for 0.025 mM PFOA in a 12 h experiment. Another report along the same lines is that by Zhang et al. [137], though in this case aqueous electrons, along with hydroxyl and other radicals, were generated by the more exotic approach of irradiating water with γ -rays. In addition to mineralization of around 86% and nearly 100% defluorination for 20 mg/L PFOA in a 22 h experiment, the report highlights the synergistic effect of hydroxyl radicals and aqueous electrons, which are both necessary to achieve efficient removal. Indeed, hydroxyl radical-based processes such as Fenton, photo-Fenton, and hydrogen peroxide activation are ineffective due to the inactivity of OH° , as also recently clarified by Javed et al. [136], who found no significant difference in PFOA degradation under UV irradiation and UV/ H_2O_2 . In contrast, several processes based on sulfate radicals ($\text{SO}_4^{\bullet-}$), obtained by persulfate activation, have been reported to be effective, though defluorination efficiencies remain low. Hori et al. used a 200 W Xe-Hg UV-visible lamp to activate persulfate (50 mM) for treating 1.35 mM PFOA in a 4 h experiment, observing an 11-fold increase in decomposition with respect to direct photolysis [138]. Similarly, Chen and Zhang used UV-activated persulfate on PFOA, reporting that while using 185 nm irradiation, decomposition was proceeded by both direct photolysis and sulfate radicals, under 254 nm light the latter was the prevalent mechanism [139]. A step forward was made by introducing ferrous iron as a persulfate activator in the system, enabling a low activation energy pathway for the decomposition of persulfate to sulfate radicals [140]. Using this approach, Tran et al. recently reported 64% degradation of PFOA (initial concentration: 1.64 μM) in a 4 h anoxic experiment [141]. However, the role of light was not clarified and defluorination not discussed, leaving room for further investigations. A further effort in this direction was made by Xu et al. [11], who combined a Ga_2O_3 photocatalyst with peroxymonosulfate as a sulfate radical sacrificial source. Under illumination from either a 32 W 185 nm light or a 32 W 254 nm light, complete degradation of a PFOA solution in the 50 ng/L to 50 mg/L range was claimed, although defluorination was not quantified. A more detailed examination of persulfate-based methods (out of the scope of this work) is being currently studied, and can be found in a recent article by Yang et al. [142]. Overall, methods based on sacrificial radical sources look promising in terms of yields, but may have similar drawbacks to direct photolysis because radical generation is often performed by activation with the same artificial UVC light sources, with all its related problems. Furthermore, the sacrificial nature of the reagents used to generate the radicals implies extra costs with respect to direct photolysis or photocatalysis. In this respect, further work is needed not only to clarify the reaction mechanisms and improve efficiency but also to evaluate the economic viability and industrial scalability of this approach with respect to current methods or other methods under study.

6. Light Sources

To date, the application of photocatalysis to PFAS compounds has mostly been performed by means of the use of artificial light sources of varying wavelengths of ultraviolet A (UVA 315–400 nm) using lamps with a light emission peak at 365 nm, and ultraviolet C (UVC 100–280 nm) using lamps with peaks at 254 and 185 nm [54]. The wavelength of 185 nm itself can degrade PFAS, since the absorption of PFOA has been confirmed for this wavelength. However, this range of wavelength at the industrial level, because of the high costs, represents a market block for AOP as a possible approach for PFAS-contaminated wastewater [133].

The employment of UVA lamps with a peak at the wavelength of 365 nm has mostly been used in systems of power ranging from 125 to 300 W in TiO₂-based photocatalysts with Pt, Pd, and Ag nanoparticles or in the presence of multi-wall carbon nanotubes (MWCNTs) [57,66]. For UVC (254 nm), studies report emission powers from 16 to 500 W for pure TiO₂, TiO₂ doped with Cu, Fe, and Pb ions, and composites with molecularly imprinted polymers. Studies have also been reported using In₂O₃ and Ga₂O₃ in sheaf, needle, microsphere, nanotube, and nanoparticle forms, as well doping with nitrogen and with CeO₂ [78,82]. Applications using ZnO have been also reported [143].

Given the present situation, an advantage could be to move towards possible photocatalysts that can absorb in the near-UV range. Indeed, by using solar concentrators, the near-UV part of the solar spectrum is reflected and focused, thus permitting its utilization with photocatalysts. Anodized aluminum mirrors with special acrylic resin coatings are interesting examples for exploiting the near-UV part of the solar spectrum [144].

7. Economic Aspects

As the applications of the advanced oxidation process seem to be in an early stage in the field of PFAS remediation, to the best of our knowledge, an in-depth analysis regarding the costs of such methodologies has not yet been published.

State agency studies report an average cost of USD 2.00/gallon for PFAS treatment when considering the combined activity of GAC and AIX (anion exchange resins) for infrastructure capacities from 2 to 50 million gallons per day (MGD) and with an initial investment from USD 3 to 120 million [145].

For budgeting PFAS management, the United States Environmental Protection Agency proposed a sequence of several necessary activities in the following order: Baseline monitoring > Public engagement > Regulatory engagement > Bench or pilot testing > Capital investment in full-scale treatment > Operation and maintenance costs of full-scale treatment > Long-term monitoring [146].

The same institution has a “Drinking water treatment technology unit cost model” and emphasizes the need for updating the model to be capable of addressing PFAS issues. The updating appears necessary because of the lack of consensus throughout the world regarding the acceptable levels of the diverse PFASs present in drinking water.

Olatunde et al. [147] undertook an economical evaluation on the applications of AOPs for degradation of PFAS substances, taking into consideration the stage of development of the technology, energy consumption, the time required to achieve 90% degradation of the substance, and the total volume of contaminated solution. Table 3 summarizes the results obtained with initial budgeting costs. The reported data show still an advantage in costs related to the use of direct photolysis, with the highest costs attributed to photocatalysis. However, the need to use radiation at a 185 nm wavelength imposes limitations to such applications in terms of lamp durability and safety. In the other hand, investments in photocatalysis research could lead to materials capable of efficiently degrading PFAS compounds with the positive feature of working under near UV-visible light.

Table 3. Relative cost comparisons between the most successful employed techniques employed for PFAS degradation (adapted from [147]).

Technology	Stage of Development	Energy (KWh/m ³)	Relative Cost (USD)	Removal Efficiency (%)	Time to 90% Degradation (min)
Photolysis (185 nm)	Emerging	99	14	82	216
Photochemicals (persulfates)	Research	864	121	99	460
Photocatalysis (indium oxides + 254 nm)	Emerging	2106	295	89	705

8. Conclusions

The degradation of PFAS substances that contaminate water represents a strong challenge for the scientific, industrial, and regulation sectors. Great efforts to develop new photocatalysts able to efficiently degrade PFAS substances have been made. However, advances are still necessary to permit the full transfer of laboratory results to field applications in wastewater treatment plants. For example, photocatalysts based on indium or gallium have scarce prospects at a large scale, while some others need to be illuminated by high-power UV emission lamps that involve large costs and a limited lifetime. However, efforts have been made to develop environmentally friendly semiconductors such as zinc and titanium-based materials that, with appropriate doping or in composites, may be activated by near UV-visible radiation, thus making use of sunlight.

A shared study that highlights the sources of PFAS pollution and their evolution, while establishing intervention strategies for the further development of efficient and low-cost photocatalysts for large-scale production that favor the use of solar radiation, will allow us to effectively provide a solution for the PFAS contamination problem. The objective of this review paper is precisely to aid in this direction.

Author Contributions: Conceptualization, D.L., M.A.F., F.P., N.P., M.O., and A.M.; writing—original draft preparation, D.L., M.A.F., F.P., N.P., M.O., and A.M.; writing—review and editing, D.L., M.A.F., F.P., N.P., M.O., and A.M.; supervision, A.M. All authors have read and agreed to the published version of the manuscript.

Funding: This research was funded by the University of Trento, project ERiCSol.

Institutional Review Board Statement: Not Applicable

Informed Consent Statement: Not Applicable

Conflicts of Interest: The authors declare no conflict of interest

References

- Buck, R.C.; Franklin, J.; Berger, U.; Conder, J.M.; Cousins, I.T.; de Voogt, P.; Jensen, A.A.; Kannan, K.; Mabury, S.A.; van Leeuwen, S.P.J. Perfluoroalkyl and polyfluoroalkyl substances in the environment: Terminology, classification, and origins. *Integr. Environ. Assess. Manag.* **2011**, *7*, 513–541, <https://doi.org/10.1002/ieam.258>.
- Baran, J.R. *Fluorinated Surfactants and Repellents*, 2nd ed.; Revised and Expanded Surfactant Science Series; *J. Am. Chem. Soc.* **2001**, *123*, 8882, doi:10.1021/ja015260a.
- Interstate Technology and Regulatory Council (ITRC), PFAS Technical and Regulatory Guidance Document and Fact. 2020. Available online: <https://pfas-1.itrcweb.org/> (accessed on 5 November 2020).
- Kirk, M.; Smurthwaite, K.; Braeunig, J.; Trevenar, S.; D'Este, C.; Lucas, R.; Lal, A.; Korda, R.; Clements, A.; Mueller, J. *The PFAS Health Study: Systematic Literature Review*; 2018. Available online: https://rsph.anu.edu.au/files/PFAS%20Health%20Study%20Systematic%20Review_1.pdf (accessed on 11 September 2021)
- Wang, S.; Yang, Q.; Chen, F.; Sun, J.; Luo, K.; Yao, F.; Wang, X.; Wang, D.; Li, X.; Zeng, G. Photocatalytic degradation of perfluorooctanoic acid and perfluorooctane sulfonate in water: A critical review. *Chem. Eng. J.* **2017**, *328*, 927–942, <https://doi.org/10.1016/j.cej.2017.07.076>.
- Xu, Y.; Fletcher, T.; Pineda, D.; Lindh, C.H.; Nilsson, C.; Glynn, A.; Vogs, C.; Norström, K.; Lilja, K.; Jakobsson, K.; et al. Serum Half-Lives for Short- and Long-Chain Perfluoroalkyl Acids after Ceasing Exposure from Drinking Water Contaminated by Firefighting Foam. *Environ. Health Perspect.* **2021**, *128*, 77004, doi:10.1289/EHP6785.

7. Peer Kirsch Front Matter. In *Modern Fluoroorganic Chemistry* **2004**, i–xii, <https://doi.org/10.1002/352760393X.fmatter>.
8. Guo, R.; Sim, W.-J.; Lee, E.-S.; Lee, J.-H.; Oh, J.-E. Evaluation of the fate of perfluoroalkyl compounds in wastewater treatment plants. *Water Res.* **2010**, *44*, 3476–3486, <https://doi.org/10.1016/j.watres.2010.03.028>.
9. Li, Z.; Zhang, P.; Shao, T.; Li, X. In₂O₃ nanoporous nanosphere: A highly efficient photocatalyst for decomposition of perfluorooctanoic acid. *Appl. Catal. B Environ.* **2012**, *125*, 350–357, <https://doi.org/10.1016/j.apcatb.2012.06.017>.
10. Li, X.; Zhang, P.; Jin, L.; Shao, T.; Li, Z.; Cao, J. Efficient Photocatalytic Decomposition of Perfluorooctanoic Acid by Indium Oxide and Its Mechanism. *Environ. Sci. Technol.* **2012**, *46*, 5528–5534, doi:10.1021/es204279u.
11. Xu, B.; Zhou, J.L.; Altaee, A.; Ahmed, M.B.; Johir, M.A.H.; Ren, J.; Li, X. Improved photocatalysis of perfluorooctanoic acid in water and wastewater by Ga₂O₃/UV system assisted by peroxymonosulfate. *Chemosphere* **2020**, *239*, 124722, <https://doi.org/10.1016/j.chemosphere.2019.124722>.
12. Henry, B.J.; Carlin, J.P.; Hammerschmidt, J.A.; Buck, R.C.; Buxton, L.W.; Fiedler, H.; Seed, J.; Hernandez, O. A critical review of the application of polymer of low concern and regulatory criteria to fluoropolymers. *Integr. Environ. Assess. Manag.* **2018**, *14*, 316–334, <https://doi.org/10.1002/ieam.4035>.
13. Lindstrom, A.B.; Strynar, M.J.; Libelo, E.L. Polyfluorinated Compounds: Past, Present, and Future. *Environ. Sci. Technol.* **2011**, *45*, 7954–7961, doi:10.1021/es2011622.
14. Washington, J.W.; Jenkins, T.M.; Rankin, K.; Naile, J.E. Decades-Scale Degradation of Commercial, Side-Chain, Fluorotelomer-Based Polymers in Soils and Water. *Environ. Sci. Technol.* **2015**, *49*, 915–923, doi:10.1021/es504347u.
15. Glüge, J.; Scheringer, M.; Cousins, I.T.; DeWitt, J.C.; Goldenman, G.; Herzke, D.; Lohmann, R.; Ng, C.A.; Trier, X.; Wang, Z. An overview of the uses of per- and polyfluoroalkyl substances (PFAS). *Environ. Sci. Process. Impacts* **2020**, *22*, 2345–2373, doi:10.1039/D0EM00291G.
16. C8 Science Panel. 2019. Available online: www.c8sciencepanel.org (accessed on 22 January 2020).
17. Emerging Chemical Risks in Europe—‘PFAS’. European Environment Agency, 12 December 2019. Last modified 9 March 2021. Available online: <https://www.eea.europa.eu/publications/emerging-chemical-risks-in-europe> (accessed on 31 March 2021), doi:10.2800/486213.
18. ATSDR. *Toxicological Profile for Perfluoroalkyls Draft for Public Comment*; US Dept. of Health and Human Sciences: Atlanta 2018. Available online: <https://www.atsdr.cdc.gov/toxprofiles/tp200.pdf> (accessed on 15 April 2021).
19. WHO. *Some Chemicals Used as Solvents and in Polymer Manufacture*; WHO, Ed.; Volume 110; IARC Monographs on the Evaluation of Carcinogenic Risks to Humans, 2016; ISBN 978-92-832-0148-9. Available online: <https://www.iarc.who.int/news-events/iarc-monographs-volume-110-some-chemicals-used-as-solvents-and-in-polymer-manufacture/> (accessed on 20 April 2021).
20. Vaughn, B.; Andrea, W.; Kyle, S. Perfluorooctanoic Acid (PFOA) Exposures and Incident Cancers among Adults Living Near a Chemical Plant. *Environ. Health Perspect.* **2013**, *121*, 1313–1318, doi:10.1289/ehp.1306615.
21. Fenton, S.E.; Reiner, J.L.; Nakayama, S.F.; Delinsky, A.D.; Stanko, J.P.; Hines, E.P.; White, S.S.; Lindstrom, A.B.; Strynar, M.J.; Petropoulou, S.-S.E. Analysis of PFOA in dosed CD-1 mice. Part 2: Disposition of PFOA in tissues and fluids from pregnant and lactating mice and their pups. *Reprod. Toxicol.* **2009**, *27*, 365–372, <https://doi.org/10.1016/j.reprotox.2009.02.012>.
22. White, S.; Stanko, P.; Kayoko, K.; M., Calafat, A.; Hines, E.P.; Fenton, S. Gestational and Chronic Low-Dose PFOA Exposures and Mammary Gland Growth and Differentiation in Three Generations of CD-1 Mice. *Environ. Health Perspect.* **2011**, *119*, 1070–1076, doi:10.1289/ehp.1002741.
23. Saleh, N.B.; Khalid, A.; Tian, Y.; Ayres, C.; Sabaraya, I.V.; Pietari, J.; Hanigan, D.; Chowdhury, I.; Apul, O.G. Removal of poly- and per-fluoroalkyl substances from aqueous systems by nano-enabled water treatment strategies. *Environ. Sci. Water Res. Technol.* **2019**, *5*, 198–208, doi:10.1039/C8EW00621K.
24. ECHA Guidance on Information Requirements and Chemical Safety Assessment, 2016. Available online: <https://echa.europa.eu/guidance-documents/guidance-on-information-requirements-and-chemical-safety-assessment> (accessed on 02/12/2020).
25. *Fourth National Report on Human Exposure to Environmental Chemicals*; 2021. Available online: https://www.cdc.gov/exposurereport/pdf/FourthReport_UpdatedTables_Volume1_Mar2021-508.pdf (accessed on 30 April 2021).
26. Meegoda, J.N.; Kewalramani, J.A.; Li, B.; Marsh, R.W. A Review of the Applications, Environmental Release, and Remediation Technologies of Per- and Polyfluoroalkyl Substances. *Int. J. Environ. Res. Public Heal.* **2020**, *17*, 8117.
27. Kucharzyk, K.H.; Darlington, R.; Benotti, M.; Deeb, R.; Hawley, E. Novel treatment technologies for PFAS compounds: A critical review. *J. Environ. Manag.* **2017**, *204*, 757–764, doi:10.1016/j.jenvman.2017.08.016.
28. Mahinroosta, R.; Senevirathna, L. A review of the emerging treatment technologies for PFAS contaminated soils. *J. Environ. Manag.* **2020**, *255*, 109896, doi:10.1016/j.jenvman.2019.109896.
29. Appleman, T.D. The removal of poly- and perfluoroalkyl substances by North American water treatment practices, Colorado School of Mines, 2012. Master’s Thesis. Available online: <http://hdl.handle.net/11124/78755> (accessed on 10 December 2020).
30. Lu, D.; Sha, S.; Luo, J.; Huang, Z.; Jackie, X.Z. Treatment train approaches for the remediation of per- and polyfluoroalkyl substances (PFAS): A critical review. *J. Hazard. Mater.* **2020**, *386*, 121963, doi:10.1016/j.jhazmat.2019.121963.
31. Wanninayake, D.M. Comparison of currently available PFAS remediation technologies in water: A review. *J. Environ. Manag.* **2021**, *283*, 111977, <https://doi.org/10.1016/j.jenvman.2021.111977>.
32. Ross, I.; McDonough, J.; Miles, J.; Storch, P.; Thelakkat Kochunarayanan, P.; Kalve, E.; Hurst, J.; Dasgupta, S.; Burdick, J. A review of emerging technologies for remediation of PFASs. *Remediat. J.* **2018**, *28*, 101–126, <https://doi.org/10.1002/rem.21553>.

33. Al Amin, M.; Sobhani, Z.; Liu, Y.; Dharmaraja, R.; Chadalavada, S.; Naidu, R.; Chalker, J.M.; Fang, C. Recent advances in the analysis of per- and polyfluoroalkyl substances (PFAS)—A review. *Environ. Technol. Innov.* **2020**, *19*, 100879, <https://doi.org/10.1016/j.eti.2020.100879>.
34. Jahnke, A.; Berger, U. Trace analysis of per- and polyfluorinated alkyl substances in various matrices—How do current methods perform? *J. Chromatogr. A* **2009**, *1216*, 410–421, <https://doi.org/10.1016/j.chroma.2008.08.098>.
35. Backe, W.J.; Day, T.C.; Field, J.A. Zwitterionic, Cationic, and Anionic Fluorinated Chemicals in Aqueous Film Forming Foam Formulations and Groundwater from U.S. Military Bases by Nonaqueous Large-Volume Injection HPLC-MS/MS. *Environ. Sci. Technol.* **2013**, *47*, 5226–5234, doi:10.1021/es3034999.
36. Kaboré, H.A.; Vo Duy, S.; Munoz, G.; Méité, L.; Desrosiers, M.; Liu, J.; Sory, T.K.; Sauvé, S. Worldwide drinking water occurrence and levels of newly-identified perfluoroalkyl and polyfluoroalkyl substances. *Sci. Total Environ.* **2018**, *616–617*, 1089–1100, <https://doi.org/10.1016/j.scitotenv.2017.10.210>.
37. Barzen-Hanson, K.A.; Field, J.A. Discovery and Implications of C2 and C3 Perfluoroalkyl Sulfonates in Aqueous Film-Forming Foams and Groundwater. *Environ. Sci. Technol. Lett.* **2015**, *2*, 95–99, doi:10.1021/acs.estlett.5b00049.
38. Yeung, L.W.Y.; Stadey, C.; Mabury, S.A. Simultaneous analysis of perfluoroalkyl and polyfluoroalkyl substances including ultrashort-chain C2 and C3 compounds in rain and river water samples by ultra performance convergence chromatography. *J. Chromatogr. A* **2017**, *1522*, 78–85, <https://doi.org/10.1016/j.chroma.2017.09.049>.
39. Shao, M.; Ding, G.; Zhang, J.; Wei, L.; Xue, H.; Zhang, N.; Li, Y.; Chen, G.; Sun, Y. Occurrence and distribution of perfluoroalkyl substances (PFASs) in surface water and bottom water of the Shuangtaizi Estuary, China. *Environ. Pollut.* **2016**, *216*, 675–681, <https://doi.org/10.1016/j.envpol.2016.06.031>.
40. Janda, J.; Nödler, K.; Brauch, H.-J.; Zwiener, C.; Lange, F.T. Robust trace analysis of polar (C2–C8) perfluorinated carboxylic acids by liquid chromatography-tandem mass spectrometry: Method development and application to surface water, groundwater and drinking water. *Environ. Sci. Pollut. Res.* **2019**, *26*, 7326–7336, doi:10.1007/s11356-018-1731-x.
41. Gellrich, V.; Brunn, H.; Stahl, T. Perfluoroalkyl and polyfluoroalkyl substances (PFASs) in mineral water and tap water. *J. Environ. Sci. Health Part A* **2013**, *48*, 129–135, doi:10.1080/10934529.2013.719431.
42. Liu, Y.; Pereira, A.D.S.; Martin, J.W. Discovery of C5–C17 Poly- and Perfluoroalkyl Substances in Water by In-Line SPE-HPLC-Orbitrap with In-Source Fragmentation Flagging. *Anal. Chem.* **2015**, *87*, 4260–4268, doi:10.1021/acs.analchem.5b00039.
43. Zhang, X.; Niu, H.; Pan, Y.; Shi, Y.; Cai, Y. Chitosan-Coated Octadecyl-Functionalized Magnetite Nanoparticles: Preparation and Application in Extraction of Trace Pollutants from Environmental Water Samples. *Anal. Chem.* **2010**, *82*, 2363–2371, doi:10.1021/ac902589t.
44. Xia, W.; Wan, Y.-J.; Wang, X.; Li, Y.; Yang, W.-J.; Wang, C.-X.; Xu, S. Sensitive bioassay for detection of PPAR α potentially hazardous ligands with gold nanoparticle probe. *J. Hazard. Mater.* **2011**, *192*, 1148–1154, <https://doi.org/10.1016/j.jhazmat.2011.06.023>.
45. Takayose, M.; Akamatsu, K.; Nawafune, H.; Murashima, T.; Matsui, J. Colorimetric Detection of Perfluorooctanoic Acid (PFOA) Utilizing Polystyrene-Modified Gold Nanoparticles. *Anal. Lett.* **2012**, *45*, 2856–2864, doi:10.1080/00032719.2012.696225.
46. Niu, H.; Wang, S.; Zhou, Z.; Ma, Y.; Ma, X.; Cai, Y. Sensitive Colorimetric Visualization of Perfluorinated Compounds Using Poly(ethylene glycol) and Perfluorinated Thiols Modified Gold Nanoparticles. *Anal. Chem.* **2014**, *86*, 4170–4177, doi:10.1021/ac403406d.
47. Wang, Z.; Cousins, I.T.; Scheringer, M.; Buck, R.C.; Hungerbühler, K. Global emission inventories for C4–C14 perfluoroalkyl carboxylic acid (PFCA) homologues from 1951 to 2030, Part I: Production and emissions from quantifiable sources. *Environ. Int.* **2014**, *70*, 62–75, <https://doi.org/10.1016/j.envint.2014.04.013>.
48. Fang, C.; Megharaj, M.; Naidu, R. Surface-enhanced Raman scattering (SERS) detection of fluorosurfactants in firefighting foams. *RSC Adv.* **2016**, *6*, 11140–11145, doi:10.1039/C5RA26114G.
49. Okaru, A.O.; Brunner, T.S.; Ackermann, S.M.; Kuballa, T.; Walch, S.G.; Kohl-Himmelseher, M.; Lachenmeier, D.W. Application of ^{19}F NMR Spectroscopy for Content Determination of Fluorinated Pharmaceuticals. *J. Anal. Methods Chem.* **2017**, *2017*, 9206297, doi:10.1155/2017/9206297.
50. Guo, W.; Jin, L.; Hu, S.; Guo, Q. Method Development for the Determination of Total Fluorine in Foods by Tandem Inductively Coupled Plasma Mass Spectrometry with a Mass-Shift Strategy. *J. Agric. Food Chem.* **2017**, *65*, 3406–3412, doi:10.1021/acs.jafc.7b00535.
51. Boča, M.; Barborik, P.; Mičušík, M.; Omastová, M. X-ray photoelectron spectroscopy as detection tool for coordinated or uncoordinated fluorine atoms demonstrated on fluoride systems NaF, K₂TaF₇, K₃TaF₈, K₂ZrF₆, Na₇Zr₆F₃₁ and K₃ZrF₇. *Solid State Sci.* **2012**, *14*, 828–832, <https://doi.org/10.1016/j.solidstatesciences.2012.04.018>.
52. Li, F.; Duan, J.; Tian, S.; Ji, H.; Zhu, Y.; Wei, Z.; Zhao, D. Short-chain per- and polyfluoroalkyl substances in aquatic systems: Occurrence, impacts and treatment. *Chem. Eng. J.* **2020**, *380*, 122506, <https://doi.org/10.1016/j.cej.2019.122506>.
53. Zhang, W.; Zhang, D.; Liang, Y. Nanotechnology in remediation of water contaminated by poly- and perfluoroalkyl substances: A review. *Environ. Pollut.* **2019**, *247*, 266–276, <https://doi.org/10.1016/j.envpol.2019.01.045>.
54. Xu, B.; Ahmed, M.B.; Zhou, J.L.; Altaee, A.; Wu, M.; Xu, G. Photocatalytic removal of perfluoroalkyl substances from water and wastewater: Mechanism, kinetics and controlling factors. *Chem. Eng. J.* **2017**, *5*, 1–9, doi:10.1016/j.chemosphere.2017.09.110.
55. Liu, X.; Wei, W.; Xu, J.; Wang, D.; Song, L.; Ni, B.-J. Photochemical decomposition of perfluorochemicals in contaminated water. *Water Res.* **2020**, *186*, 116311, <https://doi.org/10.1016/j.watres.2020.116311>.

56. Panchangam, S.C.; Lin, A.Y.-C.; Shaik, K.L.; Lin, C.-F. Decomposition of perfluorocarboxylic acids (PFCAs) by heterogeneous photocatalysis in acidic aqueous medium. *Chemosphere* **2009**, *77*, 242–248, <https://doi.org/10.1016/j.chemosphere.2009.07.003>.
57. Chen, M.-J.; Lo, S.-L.; Lee, Y.-C.; Huang, C.-C. Photocatalytic decomposition of perfluorooctanoic acid by transition-metal modified titanium dioxide. *J. Hazard. Mater.* **2015**, *288*, 168–175, <https://doi.org/10.1016/j.jhazmat.2015.02.004>.
58. Chen, Y.-C.; Lo, S.-L.; Kuo, J. Effects of titanate nanotubes synthesized by a microwave hydrothermal method on photocatalytic decomposition of perfluorooctanoic acid. *Water Res.* **2011**, *45*, 4131–4140, <https://doi.org/10.1016/j.watres.2011.05.020>.
59. Sansotera, M.; Persico, F.; Pirola, C.; Navarrini, W.; Di Michele, A.; Bianchi, C.L. Decomposition of perfluorooctanoic acid photocatalyzed by titanium dioxide: Chemical modification of the catalyst surface induced by fluoride ions. *Appl. Catal. B Environ.* **2014**, *148–149*, 29–35, <https://doi.org/10.1016/j.apcatb.2013.10.038>.
60. Wang, Y.; Zhang, P. Photocatalytic decomposition of perfluorooctanoic acid (PFOA) by TiO₂ in the presence of oxalic acid. *J. Hazard. Mater.* **2011**, *192*, 1869–1875, <https://doi.org/10.1016/j.jhazmat.2011.07.026>.
61. Song, C.; Chen, P.; Wang, C.; Zhu, L. Photodegradation of perfluorooctanoic acid by synthesized TiO₂-MWCNT composites under 365nm UV irradiation. *Chemosphere* **2012**, *86*, 853–859, [doi:10.1016/j.chemosphere.2011.11.034](https://doi.org/10.1016/j.chemosphere.2011.11.034).
62. Rivero, M.J.; Ribao, P.; Gomez-Ruiz, B.; Urtiaga, A.; Ortiz, I. Comparative performance of TiO₂-rGO photocatalyst in the degradation of dichloroacetic and perfluorooctanoic acids. *Sep. Purif. Technol.* **2020**, *240*, 116637, <https://doi.org/10.1016/j.seppur.2020.116637>.
63. Gomez-Ruiz, B.; Ribao, P.; Diban, N.; Rivero, M.J.; Ortiz, I.; Urtiaga, A. Photocatalytic degradation and mineralization of perfluorooctanoic acid (PFOA) using a composite TiO₂-rGO catalyst. *J. Hazard. Mater.* **2018**, *344*, 950–957, <https://doi.org/10.1016/j.jhazmat.2017.11.048>.
64. Zhu, C.; Xu, J.; Song, S.; Wang, J.; Li, Y.; Liu, R.; Shen, Y. TiO₂ quantum dots loaded sulfonated graphene aerogel for effective adsorption-photocatalysis of PFOA. *Sci. Total Environ.* **2020**, *698*, 134275, <https://doi.org/10.1016/j.scitotenv.2019.134275>.
65. Wu, Y.; Li, Y.; Tian, A.; Mao, K.; Liu, J. Selective Removal of Perfluorooctanoic Acid Using Molecularly Imprinted Polymer-Modified TiO₂ Nanotube Arrays. *Int. J. Photoenergy* **2016**, *2016*, 7368795, [doi:10.1155/2016/7368795](https://doi.org/10.1155/2016/7368795).
66. Li, M.; Yu, Z.; Liu, Q.; Sun, L.; Huang, W. Photocatalytic decomposition of perfluorooctanoic acid by noble metallic nanoparticles modified TiO₂. *Chem. Eng. J.* **2016**, *286*, 232–238, <https://doi.org/10.1016/j.cej.2015.10.037>.
67. Weon, S.; Suh, M.-J.; Chu, C.; Huang, D.; Stavitski, E.; Kim, J.-H. Site-Selective Loading of Single-Atom Pt on TiO₂ for Photocatalytic Oxidation and Reductive Hydrodefluorination. *ACS ES&T Eng.* **2021**, *1*, 512–522, [doi:10.1021/acsestengg.0c00210](https://doi.org/10.1021/acsestengg.0c00210).
68. Chen, M.-J.; Lo, S.-L.; Lee, Y.-C.; Kuo, J.; Wu, C.-H. Decomposition of perfluorooctanoic acid by ultraviolet light irradiation with Pb-modified titanium dioxide. *J. Hazard. Mater.* **2016**, *303*, 111–118, <https://doi.org/10.1016/j.jhazmat.2015.10.011>.
69. Li, F.; Wei, Z.; He, K.; Blaney, L.; Cheng, X.; Xu, T.; Liu, W.; Zhao, D. A concentrate-and-destroy technique for degradation of perfluorooctanoic acid in water using a new adsorptive photocatalyst. *Water Res.* **2020**, *185*, 116219, <https://doi.org/10.1016/j.watres.2020.116219>.
70. Zhu, Y.; Xu, T.; Zhao, D.; Li, F.; Liu, W.; Wang, B.; An, B. Adsorption and solid-phase photocatalytic degradation of perfluorooctane sulfonate in water using gallium-doped carbon-modified titanate nanotubes. *Chem. Eng. J.* **2021**, *421*, 129676, <https://doi.org/10.1016/j.cej.2021.129676>.
71. Abada, B.; Alivio, T.E.G.; Shao, Y.; O'Loughlin, T.E.; Klemashevich, C.; Banerjee, S.; Jayaraman, A.; Chu, K.-H. Photodegradation of fluorotelomer carboxylic 5:3 acid and perfluorooctanoic acid using zinc oxide. *Environ. Pollut.* **2018**, *243*, 637–644, <https://doi.org/10.1016/j.envpol.2018.09.023>.
72. Ong, C.B.; Mohammad, A.W.; Ng, L.Y.; Mahmoudi, E.; Azizkhani, S.; Hayati Hairom, N.H. Solar photocatalytic and surface enhancement of ZnO/rGO nanocomposite: Degradation of perfluorooctanoic acid and dye. *Process Saf. Environ. Prot.* **2017**, *112*, 298–307, <https://doi.org/10.1016/j.psep.2017.04.031>.
73. Zhao, B.; Zhang, P. Photocatalytic decomposition of perfluorooctanoic acid with β -Ga₂O₃ wide bandgap photocatalyst. *Catal. Commun.* **2009**, *10*, 1184–1187, <https://doi.org/10.1016/j.catcom.2009.01.017>.
74. Shao, T.; Zhang, P.; Li, Z.; Jin, L. Photocatalytic decomposition of perfluorooctanoic acid in pure water and wastewater by needle-like nanostructured gallium oxide. *Chin. J. Catal.* **2013**, *34*, 1551–1559, [https://doi.org/10.1016/S1872-2067\(12\)60612-3](https://doi.org/10.1016/S1872-2067(12)60612-3).
75. Shao, T.; Zhang, P.; Jin, L.; Li, Z. Photocatalytic decomposition of perfluorooctanoic acid in pure water and sewage water by nanostructured gallium oxide. *Appl. Catal. B Environ.* **2013**, *142–143*, 654–661, <https://doi.org/10.1016/j.apcatb.2013.05.074>.
76. Zhao, B.; Li, X.; Yang, L.; Wang, F.; Li, J.; Xia, W.; Li, W.; Zhou, L.; Zhao, C. β -Ga₂O₃ Nanorod Synthesis with a One-step Microwave Irradiation Hydrothermal Method and its Efficient Photocatalytic Degradation for Perfluorooctanoic Acid. *Photochem. Photobiol.* **2015**, *91*, 42–47, <https://doi.org/10.1111/php.12383>.
77. Tan, X.; Chen, G.; Xing, D.; Ding, W.; Liu, H.; Li, T.; Huang, Y. Indium-modified Ga₂O₃ hierarchical nanosheets as efficient photocatalysts for the degradation of perfluorooctanoic acid. *Environ. Sci. Nano* **2020**, *7*, 2229–2239, [doi:10.1039/D0EN00259C](https://doi.org/10.1039/D0EN00259C).
78. Li, Z.; Zhang, P.; Shao, T.; Wang, J.; Jin, L.; Li, X. Different nanostructured In₂O₃ for photocatalytic decomposition of perfluorooctanoic acid (PFOA). *J. Hazard. Mater.* **2013**, *260*, 40–46, <https://doi.org/10.1016/j.jhazmat.2013.04.042>.
79. Li, Z.; Zhang, P.; Li, J.; Shao, T.; Wang, J.; Jin, L. Synthesis of In₂O₃ porous nanoplates for photocatalytic decomposition of perfluorooctanoic acid (PFOA). *Catal. Commun.* **2014**, *43*, 42–46, <https://doi.org/10.1016/j.catcom.2013.09.004>.
80. Liu, X.; Xu, B.; Duan, X.; Hao, Q.; Wei, W.; Wang, S.; Ni, B.-J. Facile preparation of hydrophilic In₂O₃ nanospheres and rods with improved performances for photocatalytic degradation of PFOA. *Environ. Sci. Nano* **2021**, *8*, 1010–1018, [doi:10.1039/D0EN01216E](https://doi.org/10.1039/D0EN01216E).

81. Li, Z.; Zhang, P.; Li, J.; Shao, T.; Jin, L. Synthesis of In₂O₃-graphene composites and their photocatalytic performance towards perfluorooctanoic acid decomposition. *J. Photochem. Photobiol. A Chem.* **2013**, *271*, 111–116, <https://doi.org/10.1016/j.jphotochem.2013.08.012>.
82. Jiang, F.; Zhao, H.; Chen, H.; Xu, C.; Chen, J. Enhancement of photocatalytic decomposition of perfluorooctanoic acid on CeO₂/In₂O₃. *RSC Adv.* **2016**, *6*, 72015–72021, doi:10.1039/C6RA09856H.
83. Wu, Y.; Li, Y.; Fang, C.; Li, C. Highly Efficient Degradation of Perfluorooctanoic Acid over a MnO_x-Modified Oxygen-Vacancy-Rich In₂O₃ Photocatalyst. *ChemCatChem* **2019**, *11*, 2297–2303, <https://doi.org/10.1002/cctc.201900273>.
84. Xu, J.; Wu, M.; Yang, J.; Wang, Z.; Chen, M.; Teng, F. Efficient photocatalytic degradation of perfluorooctanoic acid by a wide band gap p-block metal oxyhydroxide InOOH. *Appl. Surf. Sci.* **2017**, *416*, 587–592, <https://doi.org/10.1016/j.apsusc.2017.04.040>.
85. Verma, S.; Mezgebe, B.; Sahle-Demessie, E.; Nadagouda, M.N. Photooxidative decomposition and defluorination of perfluorooctanoic acid (PFOA) using an innovative technology of UV-vis/ZnxCu_{1-x}Fe₂O₄/oxalic acid. *Chemosphere* **2021**, *280*, 130660, <https://doi.org/10.1016/j.chemosphere.2021.130660>.
86. Yang, Y.; Zhang, C.; Lai, C.; Zeng, G.; Huang, D.; Cheng, M.; Wang, J.; Chen, F.; Zhou, C.; Xiong, W. BiOX (X = Cl, Br, I) photocatalytic nanomaterials: Applications for fuels and environmental management. *Adv. Colloid Interface Sci.* **2018**, *254*, 76–93, <https://doi.org/10.1016/j.cis.2018.03.004>.
87. Song, Z.; Dong, X.; Wang, N.; Zhu, L.; Luo, Z.; Fang, J.; Xiong, C. Efficient photocatalytic defluorination of perfluorooctanoic acid over BiOCl nanosheets via a hole direct oxidation mechanism. *Chem. Eng. J.* **2017**, *317*, 925–934, <https://doi.org/10.1016/j.cej.2017.02.126>.
88. Song, Z.; Dong, X.; Fang, J.; Xiong, C.; Wang, N.; Tang, X. Improved photocatalytic degradation of perfluorooctanoic acid on oxygen vacancies-tunable bismuth oxychloride nanosheets prepared by a facile hydrolysis. *J. Hazard. Mater.* **2019**, *377*, 371–380, <https://doi.org/10.1016/j.jhazmat.2019.05.084>.
89. Wang, J.; Cao, C.; Zhang, Y.; Zhang, Y.; Zhu, L. Underneath mechanisms into the super effective degradation of PFOA by BiOF nanosheets with tunable oxygen vacancies on exposed (101) facets. *Appl. Catal. B Environ.* **2021**, *286*, 3–5, doi:10.1016/j.apcatb.2021.119911.
90. Li, T.; Wang, C.; Wang, T.; Zhu, L. Highly efficient photocatalytic degradation toward perfluorooctanoic acid by bromine doped BiOI with high exposure of (001) facet. *Appl. Catal. B Environ.* **2020**, *268*, 118442, doi:10.1016/j.apcatb.2019.118442.
91. Wang, J.; Wang, Y.; Cao, C.; Zhang, Y.; Zhang, Y.; Zhu, L. Decomposition of highly persistent perfluorooctanoic acid by hollow Bi/BiOI_{1-x}F_x: Synergistic effects of surface plasmon resonance and modified band structures. *J. Hazard. Mater.* **2021**, *402*, 123459, <https://doi.org/10.1016/j.jhazmat.2020.123459>.
92. Wang, J.; Cao, C.; Wang, Y.; Wang, Y.; Sun, B.; Zhu, L. In situ preparation of p-n BiOI@Bi₅O₇I heterojunction for enhanced PFOA photocatalytic degradation under simulated solar light irradiation. *Chem. Eng. J.* **2020**, *391*, 123530, <https://doi.org/10.1016/j.cej.2019.123530>.
93. Yang, Y.; Ji, W.; Li, X.; Zheng, Z.; Bi, F.; Yang, M.; Xu, J.; Zhang, X. Insights into the degradation mechanism of perfluorooctanoic acid under visible-light irradiation through fabricating flower-shaped Bi₅O₇I/ZnO n-n heterojunction microspheres. *Chem. Eng. J.* **2021**, *420*, 129934, <https://doi.org/10.1016/j.cej.2021.129934>.
94. Sahu, S.P.; Qanbarzadeh, M.; Ateia, M.; Torkzadeh, H.; Maroli, A.S.; Cates, E.L. Rapid Degradation and Mineralization of Perfluorooctanoic Acid by a New Petitjeanite Bi₃O(OH)(PO₄)₂ Microparticle Ultraviolet Photocatalyst. *Environ. Sci. Technol. Lett.* **2018**, *5*, 533–538, doi:10.1021/acs.estlett.8b00395.
95. Xu, T.; Zhu, Y.; Duan, J.; Xia, Y.; Tong, T.; Zhang, L.; Zhao, D. Enhanced photocatalytic degradation of perfluorooctanoic acid using carbon-modified bismuth phosphate composite: Effectiveness, material synergy and roles of carbon. *Chem. Eng. J.* **2020**, *395*, 124991, <https://doi.org/10.1016/j.cej.2020.124991>.
96. Xu, T.; Ji, H.; Gu, Y.; Tong, T.; Xia, Y.; Zhang, L.; Zhao, D. Enhanced adsorption and photocatalytic degradation of perfluorooctanoic acid in water using iron (hydr)oxides/carbon sphere composite. *Chem. Eng. J.* **2020**, *388*, 124230, <https://doi.org/10.1016/j.cej.2020.124230>.
97. Duan, L.; Wang, B.; Heck, K.; Guo, S.; Clark, C.A.; Arredondo, J.; Wang, M.; Senftle, T.P.; Westerhoff, P.; Wen, X.; et al. Efficient Photocatalytic PFOA Degradation over Boron Nitride. *Environ. Sci. Technol. Lett.* **2020**, *7*, 613–619, doi:10.1021/acs.estlett.0c00434.
98. You, X.; Yu, L.; Xiao, F.; Wu, S.; Yang, C.; Cheng, J. Synthesis of phosphotungstic acid-supported bimodal mesoporous silica-based catalyst for defluorination of aqueous perfluorooctanoic acid under vacuum UV irradiation. *Chem. Eng. J.* **2018**, *335*, 812–821, <https://doi.org/10.1016/j.cej.2017.10.123>.
99. Tang, H.; Zhang, W.; Meng, Y.; Xia, S. A direct Z-scheme heterojunction with boosted transportation of photogenerated charge carriers for highly efficient photodegradation of PFOA: Reaction kinetics and mechanism. *Appl. Catal. B Environ.* **2021**, *285*, 119851, <https://doi.org/10.1016/j.apcatb.2020.119851>.
100. Banks, D.; Jun, B.-M.; Heo, J.; Her, N.; Park, C.M.; Yoon, Y. Selected advanced water treatment technologies for perfluoroalkyl and polyfluoroalkyl substances: A review. *Sep. Purif. Technol.* **2020**, *231*, 115929, <https://doi.org/10.1016/j.seppur.2019.115929>.
101. Xu, B.; Liu, S.; Zhou, J.L.; Zheng, C.; Weifeng, J.; Chen, B.; Zhang, T.; Qiu, W. PFAS and their substitutes in groundwater: Occurrence, transformation and remediation. *J. Hazard. Mater.* **2021**, *412*, 125159, <https://doi.org/10.1016/j.jhazmat.2021.125159>.
102. Merino, N.; Qu, Y.; Deeb, R.A.; Hawley, E.L.; Hoffmann, M.R.; Mahendra, S. Degradation and Removal Methods for Perfluoroalkyl and Polyfluoroalkyl Substances in Water. *Environ. Eng. Sci.* **2016**, *33*, 615–649, doi:10.1089/ees.2016.0233.

103. Ahmed, M.B.; Alam, M.M.; Zhou, J.L.; Xu, B.; Johir, M.A.H.; Karmakar, A.K.; Rahman, M.S.; Hossen, J.; Hasan, A.T.M.K.; Moni, M.A. Advanced treatment technologies efficacies and mechanism of per- and poly-fluoroalkyl substances removal from water. *Process Saf. Environ. Prot.* **2020**, *136*, 1–14, <https://doi.org/10.1016/j.psep.2020.01.005>.
104. Gatto, S.; Sansotera, M.; Persico, F.; Gola, M.; Pirola, C.; Panzeri, W.; Navarrini, W.; Bianchi, C.L. Surface fluorination on TiO₂ catalyst induced by photodegradation of perfluorooctanoic acid. *Catal. Today* **2015**, *241*, 8–14, <https://doi.org/10.1016/j.cattod.2014.04.031>.
105. Parrino, F.; De Pasquale, C.; Palmisano, L. Influence of Surface-Related Phenomena on Mechanism, Selectivity, and Conversion of TiO₂-Induced Photocatalytic Reactions. *ChemSusChem* **2019**, *12*, 589–602, <https://doi.org/10.1002/cssc.201801898>.
106. Zaggia, A.; Ameduri, B. Recent advances on synthesis of potentially non-bioaccumulable fluorinated surfactants. *Curr. Opin. Colloid Interface Sci.* **2012**, *17*, 188–195, <https://doi.org/10.1016/j.cocis.2012.04.001>.
107. Panchangam, S.C.; Lin, A.Y.-C.; Tsai, J.-H.; Lin, C.-F. Sonication-assisted photocatalytic decomposition of perfluorooctanoic acid. *Chemosphere* **2009**, *75*, 654–660, <https://doi.org/10.1016/j.chemosphere.2008.12.065>.
108. Lin, H.; Niu, J.; Ding, S.; Zhang, L. Electrochemical degradation of perfluorooctanoic acid (PFOA) by Ti/SnO₂-Sb, Ti/SnO₂-Sb/PbO₂ and Ti/SnO₂-Sb/MnO₂ anodes. *Water Res.* **2012**, *46*, 2281–2289, <https://doi.org/10.1016/j.watres.2012.01.053>.
109. Kutsuna, S.; Hori, H. Rate constants for aqueous-phase reactions of SO₄⁻ with C₂F₅C(O)O⁻ and C₃F₇C(O)O⁻ at 298 K. *Int. J. Chem. Kinet.* **2007**, *39*, 276–288, <https://doi.org/10.1002/kin.20239>.
110. Talaemashhadi, S.; Sansotera, M.; Gambarotti, C.; Famulari, A.; Bianchi, C.L.; Antonio Guarda, P.; Navarrini, W. Functionalization of multi-walled carbon nanotubes with perfluoropolyether peroxide to produce superhydrophobic properties. *Carbon N. Y.* **2013**, *59*, 150–159, <https://doi.org/10.1016/j.carbon.2013.03.003>.
111. de Bruyn, W.J.; Shorter, J.A.; Davidovits, P.; Worsnop, D.R.; Zahniser, M.S.; Kolb, C.E. Uptake of Haloacetyl and Carbonyl Halides by Water Surfaces. *Environ. Sci. Technol.* **1995**, *29*, 1179–1185, doi:10.1021/es00005a007.
112. Sansotera, M.; Navarrini, W.; Gola, M.; Bianchi, C.L.; Wormald, P.; Famulari, A.; Avataneo, M. Peroxidic perfluoropolyether for the covalent binding of perfluoropolyether chains on carbon black surface. *J. Fluor. Chem.* **2011**, *132*, 1254–1261, <https://doi.org/10.1016/j.jfluchem.2011.07.018>.
113. Wallington, T.J.; Ellermann, T.; Nielsen, O.J.; Sehested, J. Atmospheric Chemistry of FCO_x Radicals: UV Spectra and Self-Reaction Kinetics of FCO and FC(O)O₂ and Kinetics of Some Reactions of FCO_x with O₂, O₃, and NO at 296 K. *J. Phys. Chem.* **1994**, *98*, 2346–2356, doi:10.1021/j100060a024.
114. Sansotera, M.; Navarrini, W.; Magagnin, L.; Bianchi, C.L.; Sanguineti, A.; Metrangolo, P.; Resnati, G. Hydrophobic carbonaceous materials obtained by covalent bonding of perfluorocarbon and perfluoropolyether chains. *J. Mater. Chem.* **2010**, *20*, 8607–8616, doi:10.1039/C0JM02077J.
115. Giri, R.R.; Ozaki, H.; Morigaki, T.; Taniguchi, S.; Takanami, R. UV photolysis of perfluorooctanoic acid (PFOA) in dilute aqueous solution. *Water Sci. Technol.* **2011**, *63*, 276–282, doi:10.2166/wst.2011.050.
116. Hori, H.; Hayakawa, E.; Einaga, H.; Kutsuna, S.; Koike, K.; Ibusuki, T.; Kiatagawa, H.; Arakawa, R. Decomposition of Environmentally Persistent Perfluorooctanoic Acid in Water by Photochemical Approaches. *Environ. Sci. Technol.* **2004**, *38*, 6118–6124, doi:10.1021/es049719n.
117. Cao, M.H.; Wang, B.B.; Yu, H.S.; Wang, L.L.; Yuan, S.H.; Chen, J. Photochemical decomposition of perfluorooctanoic acid in aqueous periodate with VUV and UV light irradiation. *J. Hazard. Mater.* **2010**, *179*, 1143–1146, <https://doi.org/10.1016/j.jhazmat.2010.02.030>.
118. Vecitis, C.D.; Park, H.; Cheng, J.; Mader, B.T.; Hoffmann, M.R. Treatment technologies for aqueous perfluorooctanesulfonate (PFOS) and perfluorooctanoate (PFOA). *Front. Environ. Sci. Eng. China* **2009**, *3*, 129–151, doi:10.1007/s11783-009-0022-7.
119. Dillert, R.; Bahnemann, D.; Hidaka, H. Light-induced degradation of perfluorocarboxylic acids in the presence of titanium dioxide. *Chemosphere* **2007**, *67*, 785–792, <https://doi.org/10.1016/j.chemosphere.2006.10.023>.
120. Choi, W.; Hoffmann, M.R. Novel Photocatalytic Mechanisms for CHCl₃, CHBr₃, and CCl₃CO₂⁻ Degradation and the Fate of Photogenerated Trihalomethyl Radicals on TiO₂. *Environ. Sci. Technol.* **1997**, *31*, 89–95, doi:10.1021/es960157k.
121. Fessi, N.; Nsib, M.F.; Cardenas, L.; Guillard, C.; Dappozze, F.; Houas, A.; Parrino, F.; Palmisano, L.; Ledoux, G.; Amans, D.; et al. Surface and Electronic Features of Fluorinated TiO₂ and Their Influence on the Photocatalytic Degradation of 1-Methylnaphthalene. *J. Phys. Chem. C* **2020**, *124*, 11456–11468, doi:10.1021/acs.jpcc.0c01929.
122. Schröder, H.F.; Meesters, R.J.W. Stability of fluorinated surfactants in advanced oxidation processes—A follow up of degradation products using flow injection–mass spectrometry, liquid chromatography–mass spectrometry and liquid chromatography–multiple stage mass spectrometry. *J. Chromatogr. A* **2005**, *1082*, 110–119, <https://doi.org/10.1016/j.chroma.2005.02.070>.
123. Yang, S.; Wang, P.; Yang, X.; Shan, L.; Zhang, W.; Shao, X.; Niu, R. Degradation efficiencies of azo dye Acid Orange 7 by the interaction of heat, UV and anions with common oxidants: Persulfate, peroxymonosulfate and hydrogen peroxide. *J. Hazard. Mater.* **2010**, *179*, 552–558, <https://doi.org/10.1016/j.jhazmat.2010.03.039>.
124. Zhao, D.; Liao, X.; Yan, X.; Huling, S.G.; Chai, T.; Tao, H. Effect and mechanism of persulfate activated by different methods for PAHs removal in soil. *J. Hazard. Mater.* **2013**, *254–255*, 228–235, <https://doi.org/10.1016/j.jhazmat.2013.03.056>.
125. Santos, A.; Rodríguez, S.; Pardo, F.; Romero, A. Use of Fenton reagent combined with humic acids for the removal of PFOA from contaminated water. *Sci. Total Environ.* **2016**, *563–564*, 657–663, <https://doi.org/10.1016/j.scitotenv.2015.09.044>.
126. Yang, S.; Cheng, J.; Sun, J.; Hu, Y.; Liang, X. Defluorination of Aqueous Perfluorooctanesulfonate by Activated Persulfate Oxidation. *PLoS ONE* **2013**, *8*, e74877.

127. Lee, Y.-C.; Lo, S.-L.; Chiueh, P.-T.; Liou, Y.-H.; Chen, M.-L. Microwave-hydrothermal decomposition of perfluorooctanoic acid in water by iron-activated persulfate oxidation. *Water Res.* **2010**, *44*, 886–892, <https://doi.org/10.1016/j.watres.2009.09.055>.
128. Lee, Y.; Lo, S.; Kuo, J.; Hsieh, C. Decomposition of perfluorooctanoic acid by microwave-activated persulfate: Effects of temperature, pH, and chloride ions. *Front. Environ. Sci. Eng.* **2012**, *6*, 17–25, doi:10.1007/s11783-011-0371-x.
129. Kim, T.-H.; Lee, S.-H.; Kim, H.Y.; Doudrick, K.; Yu, S.; Kim, S.D. Decomposition of perfluorooctane sulfonate (PFOS) using a hybrid process with electron beam and chemical oxidants. *Chem. Eng. J.* **2019**, *361*, 1363–1370, <https://doi.org/10.1016/j.cej.2018.10.195>.
130. Taniyasu, S.; Yamashita, N.; Yamazaki, E.; Petrick, G.; Kannan, K. The environmental photolysis of perfluorooctanesulfonate, perfluorooctanoate, and related fluorochemicals. *Chemosphere* **2013**, *90*, 1686–1692, <https://doi.org/10.1016/j.chemosphere.2012.09.065>.
131. Qu, Y.; Zhang, C.; Li, F.; Chen, J.; Zhou, Q. Photo-reductive defluorination of perfluorooctanoic acid in water. *Water Res.* **2010**, *44*, 2939–2947, <https://doi.org/10.1016/j.watres.2010.02.019>.
132. Giri, R.R.; Ozaki, H.; Okada, T.; Taniguchi, S.; Takanami, R. Factors influencing UV photodecomposition of perfluorooctanoic acid in water. *Chem. Eng. J.* **2012**, *180*, 197–203, <https://doi.org/10.1016/j.cej.2011.11.049>.
133. Chen, J.; Zhang, P.; Liu, J. Photodegradation of perfluorooctanoic acid by 185 nm vacuum ultraviolet light. *J. Environ. Sci.* **2007**, *19*, 387–390, doi:10.1016/S1001-0742(07)60064-3.
134. Hori, H.; Yamamoto, A.; Koike, K.; Kutsuna, S.; Osaka, I.; Arakawa, R. Photochemical decomposition of environmentally persistent short-chain perfluorocarboxylic acids in water mediated by iron(II)/(III) redox reactions. *Chemosphere* **2007**, *68*, 572–578, <https://doi.org/10.1016/j.chemosphere.2006.12.038>.
135. Chen, Z.; Teng, Y.; Mi, N.; Jin, X.; Yang, D.; Wang, C.; Wu, B.; Ren, H.; Zeng, G.; Gu, C. Highly Efficient Hydrated Electron Utilization and Reductive Destruction of Perfluoroalkyl Substances Induced by Intermolecular Interaction. *Environ. Sci. Technol.* **2021**, *55*, 3996–4006, doi:10.1021/acs.est.0c07927.
136. Javed, H.; Lyu, C.; Sun, R.; Zhang, D.; Alvarez, P.J.J. Discerning the inefficacy of hydroxyl radicals during perfluorooctanoic acid degradation. *Chemosphere* **2020**, *247*, 125883, <https://doi.org/10.1016/j.chemosphere.2020.125883>.
137. Zhang, Z.; Chen, J.-J.; Lyu, X.-J.; Yin, H.; Sheng, G.-P. Complete mineralization of perfluorooctanoic acid (PFOA) by γ -irradiation in aqueous solution. *Sci. Rep.* **2014**, *4*, 7418, doi:10.1038/srep07418.
138. Hori, H.; Yamamoto, A.; Hayakawa, E.; Taniyasu, S.; Yamashita, N.; Kutsuna, S.; Kiatagawa, H.; Arakawa, R. Efficient Decomposition of Environmentally Persistent Perfluorocarboxylic Acids by Use of Persulfate as a Photochemical Oxidant. *Environ. Sci. Technol.* **2005**, *39*, 2383–2388, doi:10.1021/es0484754.
139. Chen, J.; Zhang, P. Photodegradation of perfluorooctanoic acid in water under irradiation of 254 nm and 185 nm light by use of persulfate. *Water Sci. Technol.* **2006**, *54*, 317–325, doi:10.2166/wst.2006.731.
140. Liang, C.; Bruell, C.J.; Marley, M.C.; Sperry, K.L. Persulfate oxidation for in situ remediation of TCE. I. Activated by ferrous ion with and without a persulfate–thiosulfate redox couple. *Chemosphere* **2004**, *55*, 1213–1223, <https://doi.org/10.1016/j.chemosphere.2004.01.029>.
141. Tran, T.; Abrell, L.; Brusseau, M.L.; Chorover, J. Iron-activated persulfate oxidation degrades aqueous Perfluorooctanoic acid (PFOA) at ambient temperature. *Chemosphere* **2021**, *281*, 130824, <https://doi.org/10.1016/j.chemosphere.2021.130824>.
142. Yang, L.; He, L.; Xue, J.; Ma, Y.; Xie, Z.; Wu, L.; Huang, M.; Zhang, Z. Persulfate-based degradation of perfluorooctanoic acid (PFOA) and perfluorooctane sulfonate (PFOS) in aqueous solution: Review on influences, mechanisms and prospective. *J. Hazard. Mater.* **2020**, *393*, 122405, <https://doi.org/10.1016/j.jhazmat.2020.122405>.
143. Wu, D.; Li, X.; Tang, Y.; Lu, P.; Chen, W.; Xu, X.; Li, L. Mechanism insight of PFOA degradation by ZnO assisted-photocatalytic ozonation: Efficiency and intermediates. *Chemosphere* **2017**, *180*, 247–252, doi:10.1016/j.chemosphere.2017.03.127.
144. Malato, S.; Fernández-Ibáñez, P.; Maldonado, M.I.; Blanco, J.; Gernjak, W. Decontamination and disinfection of water by solar photocatalysis: Recent overview and trends. *Catal. Today* **2009**, *147*, 1–59, <https://doi.org/10.1016/j.cattod.2009.06.018>.
145. National Association of Clean Water Agencies (NACWA). Available online: <https://www.nacwa.org/> (accessed on 22 January 2021).
146. Whitby, P.; Yu, R.; Mackey, E. Consider the Hidden Costs of PFAS Treatment. *Opflow* **2021**, *47*, 10–15, <https://doi.org/10.1002/opfl.1484>.
147. Olatunde, O.C.; Kuvarega, A.T.; Onwudiwe, D.C. Photo enhanced degradation of polyfluoroalkyl and perfluoroalkyl substances. *Heliyon* **2020**, *6*, e05614, <https://doi.org/10.1016/j.heliyon.2020.e05614>.